AGU PUBLICATIONS

Paleoceanography

RESEARCH ARTICLE
10.1002/2015PA002906

Key Points:
- Global deepwater circulation regime between 2.4 and 1.7 Ma is reconstructed
- NADW ventilated most of the ocean interior, while AABW was isolated
- AABW-NADW salinity gradient reversal preconditioned this regime

Supporting Information:
- Supporting Information S1
- Data Set S1

Correspondence to:
B. Huang,
bqhuang@pku.edu.cn

Citation:
Du, J., B. Huang, and L. Zhou (2016), Global deepwater circulation between 2.4 and 1.7 Ma and its connection to the onset of Northern Hemisphere Glaciation, *Paleoceanography*, *31*, 1480–1497, doi:10.1002/2015PA002906.

Received 20 NOV 2015
Accepted 3 OCT 2016
Accepted article online 5 OCT 2016
Published online 3 NOV 2016

Global deepwater circulation between 2.4 and 1.7 Ma and its connection to the onset of Northern Hemisphere Glaciation

Jianghui Du[1], Baoqi Huang[2,3], and Liping Zhou[4,5]

[1]College of Earth, Ocean, and Atmospheric Sciences, Oregon State University, Corvallis, Oregon, USA, [2]The Laboratory of Orogenic Belts and Crustal Evolution, Ministry of Education, Peking University, Beijing, China, [3]School of Earth and Space Sciences, Peking University, Beijing, China, [4]Department of Geography, Peking University, Beijing, China, [5]Institute of Ocean Research, Peking University, Beijing, China

Abstract We have generated an early Pleistocene benthic isotopic record for the Ocean Drilling Program Site 807 (2804 m) from the western equatorial Pacific. Between 2.4 and 1.7 Ma, the benthic $\delta^{13}C$ of this site and a few other deep Pacific sites was consistently higher than the Southern Ocean Site MV0502-4JC (4286 m), pointing to a reversal relative to the current gradient and hence implying a different circulation regime. We reconstructed the deepwater mass distribution of this interval by using a collection of benthic isotope records from 15 Pacific and 10 Atlantic sites and a $\delta^{13}C$-$\delta^{18}O$ mixing model. A two-end-member mixing regime between the North Atlantic Deep Water (NADW) and the Antarctic Bottom Water (AABW), with properties very different from today, was identified. The Southern Ocean showed strong signs of stratification and AABW with low benthic $\delta^{13}C$, but high $\delta^{18}O$ values reached out to other basins only below ~4000 m. In contrast, NADW ventilated most of the ocean interior, contributing ~70% to the Pacific Deep Water volumetrically. Our model results also reveal a strong remineralization effect at the bottom sites of the Pacific and the Atlantic, suggesting significant accumulation of respired carbon in the bottom water between 2.4 and 1.7 Ma. We propose that such a circulation pattern was initiated by the reversal of salinity gradient between AABW and NADW from 3.0 to 2.4 Ma, possibly linked to Antarctic sea ice expansion and reduced southward heat transport during the onset of Northern Hemisphere Glaciation.

1. Introduction

Deep water circulation, because of its significant impact on the global distributions of heat, carbon, and nutrients, is featured in a prominent role in paleoclimate research. Previous studies have extensively documented its regime shifts on different time scales in the late Pleistocene, and how such shifts were related to global climate change, such as the abrupt climate events on millennial time scale and the variation of atmospheric CO_2 level on orbital time scale [e.g., *Broecker*, 1997, 2003; *Clark et al*., 2002; *Knox and McElroy*, 1984; *Rahmstorf*, 2002; *Sarmiento and Toggweiler*, 1984; *Siegenthaler and Wenk*, 1984; *Sigman and Boyle*, 2000]. In contrast, relatively less is known about what the circulation regime was and what role it played during the Plio-Pleistocene climate transition, which saw the onset of Northern Hemisphere Glaciation (NHG) [*Fedorov et al*., 2013; *Mix et al*., 1995b; *Mudelsee and Raymo*, 2005; *Raymo*, 1994; *Sarnthein et al*., 2009]. It has been demonstrated that during this transition middle- and high-latitude sea surface and bottom water temperature (SST and BWT) declined worldwide, zonal and meridional gradients of SST built up in the Pacific, Hadley and Walker circulation strengthened, coastal and equatorial upwelling system intensified, the level of atmospheric CO_2 dropped, and the subpolar North Pacific and the Southern Ocean became stratified [*Bartoli et al*., 2011; *Brierley and Fedorov*, 2010; *Etourneau et al*., 2010; *Fedorov et al*., 2013; *Haug et al*., 1999; *Sigman et al*., 2004; *Wara et al*., 2005]. Accompanying these atmospheric and surface ocean trends was the reconfiguration of deep ocean circulation [*Raymo*, 1994; *Raymo et al*., 1992, 1990, 1989], one prominent aspect of which was indicated by the excursion of deep (>3500 m) Southern Ocean benthic $\delta^{13}C$ toward lower values, traditionally interpreted as the result of the suppression of NADW or the isolation of Southern Ocean deepwater masses [*Hodell and Venz-Curtis*, 2006; *Raymo et al*., 1992; *Venz and Hodell*, 2002; *Waddell et al*., 2009].

An example of this negative excursion was that between 2.7 and 1.55 Ma the benthic $\delta^{13}C$ of Southern Ocean Ocean Drilling Program (ODP) Site 1090 (3702 m) approached, though rarely dropped below, the Pacific Site 849 (3851 m) [*Hodell and Venz-Curtis*, 2006]. Moreover, when comparing a deeper Southern Ocean site

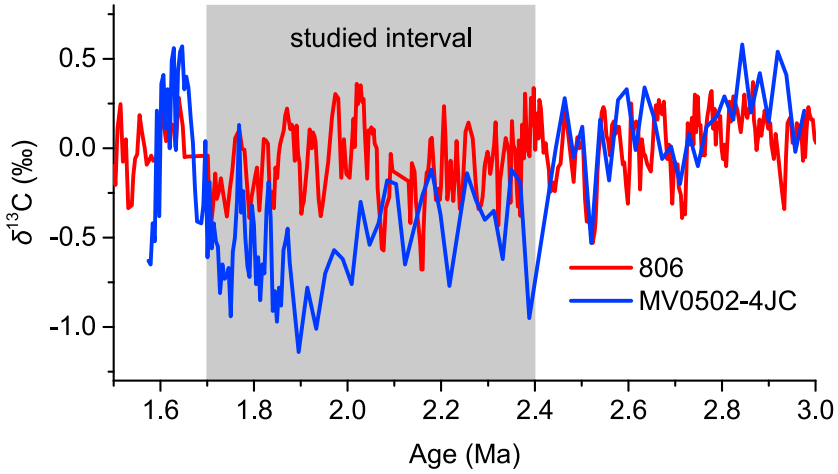

Figure 1. Comparison of benthic $\delta^{13}C$ record of Southern Ocean Site MV0502-4JC [*Waddell et al*., 2009] with Pacific Sites 807 (this study) and 806 [*Bickert et al*., 1997; *Karas et al*., 2009].

MV0502-4JC (4286 m) [*Waddell et al*., 2009] with a shallower Pacific Site 806 (2520 m) [*Bickert et al*., 1997; *Karas et al*., 2009], which presumably are situated at better depth ranges to represent their respective water masses (Antarctic Bottom Water (AABW) and Pacific Deep Water (PDW)), we find this negative excursion culminated in the benthic $\delta^{13}C$ of AABW being consistently lower than PDW between 2.4 and 1.7 Ma for ~0.7 Ma (Figure 1). The drop of deep Southern Ocean benthic $\delta^{13}C$ below the Pacific value is not uncommon during the late Pleistocene glacial maxima [e.g., *Lisiecki*, 2010] and is usually considered to reflect poor ventilation of the deep Southern Ocean [*Hodell et al*., 2003a]. However, it has not been documented before in the Plio-Pleistocene climate history that such a situation could last so long and exist regardless of glacial-interglacial cycles. In this study, we reconstruct the global deepwater circulation regime of this interval (2.4–1.7 Ma) and investigate what initiated this circulation pattern and how it was related to the onset of NHG. Our method is using a collection of benthic stable carbon and oxygen isotope data from 25 sites globally and a $\delta^{13}C$-$\delta^{18}O$ mixing model to map deepwater mass distribution.

2. Materials and Methods

2.1. Site Selection

Only sites from studies that primarily use *Cibicidoides* for stable isotope analyses in the 2.4–1.7 Ma interval are selected. One exception is made because this deep Pacific site (V28-179, 4509 m) is geographically important in filling the gaps of water mass distribution (Figure 2). We also prefer open ocean sites, but to close vertical gaps we do include sites from the marginal basins, and they are used to represent open ocean conditions at their respective sill depths if they are beneath such depth levels. In summary, there are 11 North and Equatorial Pacific sites, 7 North and Equatorial Atlantic sites, and 7 South Pacific and South Atlantic sites in the collection. Among them only one is not based on *Cibicidoides* and four are from the marginal seas (three from the South China Sea (SCS) and two of which are beneath the sill depth; another one is from the Caribbean Sea). The circumpolar nature of the Southern Ocean water masses makes it reasonable to group the South Atlantic and South Pacific sites together, the validity of which will be further discussed in section 3.1.1. Site information and references are listed in Table 1, and site map can be found in Figure 2. A brief introduction to these sites is included in Text S1 in the supporting information (*Bickert et al*. [1997], *Haug and Tiedemann* [1998], *Hodell and Venz-Curtis* [2006], *MacCready et al*. [1999], *Mix et al*. [1995a], *Wang and Li* [2009], and references in Table 1). It is useful to mention that by 2.5 Ma the Central American Seaway had been fully closed [*Sarnthein et al*., 2009], and this is the last major tectonic event that might have affected the configuration of global deepwater circulation.

2.2. Benthic Isotopes

Along with this suite of sites we also produced a new benthic isotopic record from ODP Site 807 located on the Ontong Java Plateau. Sediments from Site 807 Hole A were sampled at 5–10 cm intervals for the early

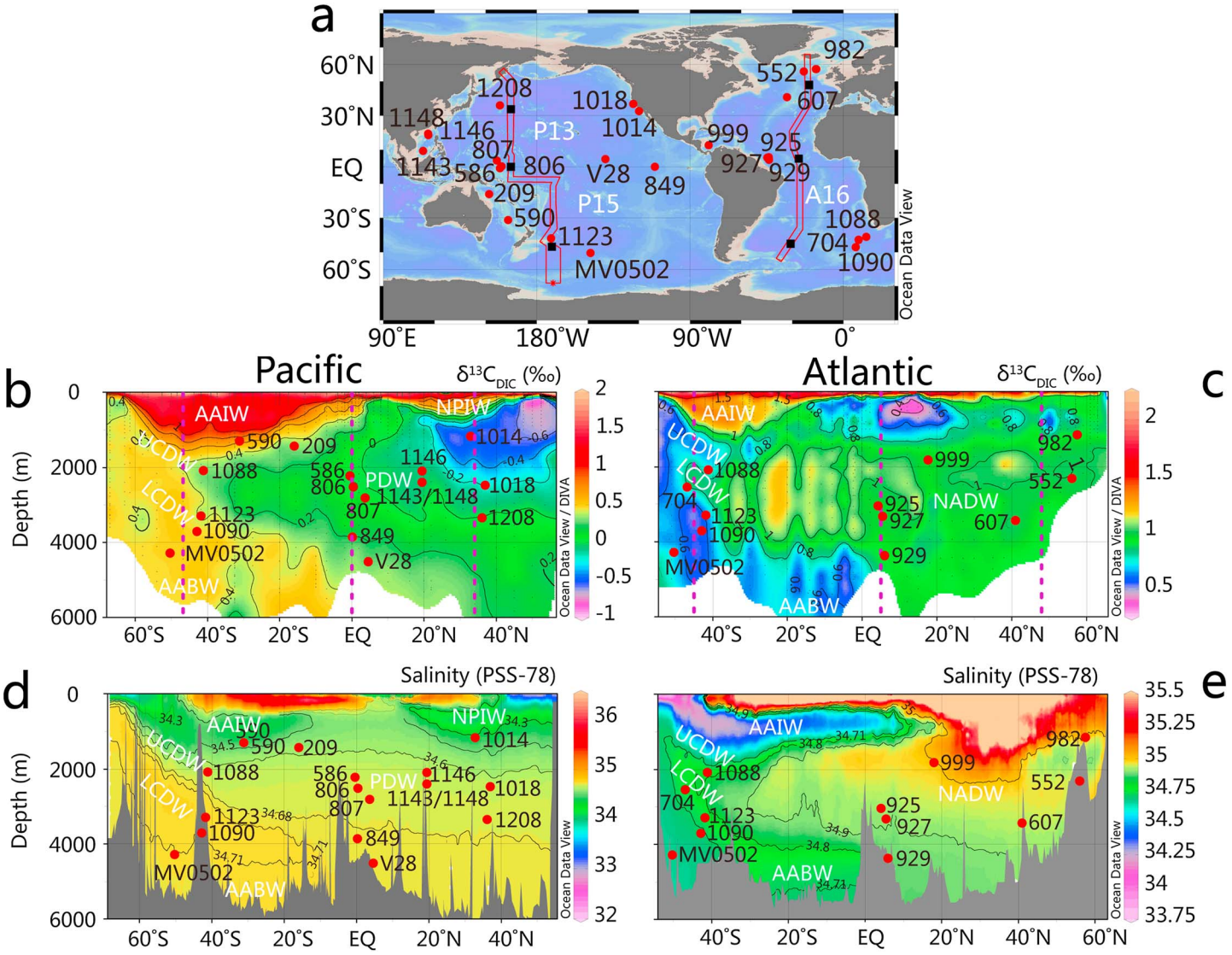

Figure 2. (a) Site locations and modern meridional distributions of $\delta^{13}C_{DIC}$ and salinity in the (b and d) Pacific and (c and e) Atlantic Ocean. The $\delta^{13}C_{DIC}$ data are from *Schmittner et al.* [2013] and salinity data from GLODAP [*Key et al.*, 2004]. The Pacific section is a combination of the World Ocean Circulation Experiment P13 and the southern part of P15. The Atlantic section is A16. Detailed site information can be found in Table 1 and Text S1. Water masses are noted in the figure and described in Text S4. The six black filled squares in Figure 2a and the six purple dash lines in Figures 2b and 2c indicate locations of modern vertical $\delta^{13}C_{DIC}$ profiles used in Figure 4. In the figures, V28 is short for V28-179 and MV0502 for MV0502-4JC. Note that Sites 704, 1088, and 1090 in the South Atlantic are also plotted in Figures 2b and 2d for comparison with the South Pacific sites. So are the South Pacific Site ODP 1123 and MV0502-4JC in Figures 2c and 2e. Figures are created by using the Ocean Data View program [*Schlitzer*, 2014].

Pleistocene based on a published age model [*Jin et al.*, 2011]. Isotopic analyses were conducted on 2–7 specimens of *Cibicidoides wuellerstorfi* in the >154 μm size fraction. Analyses were conducted at the State Key Laboratory of Marine Geology at Tongji University on a Finnigan MAT 252 Mass Spectrometer (Kiel II), and the results were reported relative to the Pee Dee belemnite (PDB) standard. Analytical precision, based on the laboratory's replicate measurements of the NBS19 standard, was ±0.07‰ for $\delta^{18}O$ and ±0.04‰ for $\delta^{13}C$ (1σ). Coupled measurements of the $\delta^{13}C$ of dissolved inorganic carbon ($\delta^{13}C_{DIC}$) and core top *C. wuellerstorfi* samples suggested this species "*faithfully records bottom water* $\delta^{13}C$" at the Ontong Java Plateau [*McCorkle and Keigwin*, 1994].

V28-179 is the only site in which the benthic species used was not *Cibicidoides* but *Globocassidulina subglobosa*. We add 0.5‰ to its $\delta^{13}C$ and subtract 0.1‰ from its $\delta^{18}O$ according to the isotopic adjustment factors in *Shackleton and Hall* [1984]. For all the other sites, non-*Cibicidoides* data are excluded. The $\delta^{18}O$ data of

Table 1. Information of Collected Sites Used in This Study

Site	Latitude	Longitude	Depth (m)	Water Mass	Age Model[a]	N[b]	Reference
				North Pacific			
1014	32°50′N	119°58′W	1165	NPIW/PDW	LR04M&B	47	*Kwiek and Ravelo* [1999]
1146	19°27′N	116°16′E	2092	PDW/SCS	LR04	209	*Clemens et al.* [2008]
1018	36°59′N	123°17′W	2476	PDW	LR04B	14	*Kwiek and Ravelo* [1999]
1143[c]	9°22′N	113°17′E	2772	PDW/SCS	LR04	199	*Cheng et al.* [2004a]
1148[c]	18°50′N	116°34′E	3294	PDW/SCS	Other	85	*Cheng et al.* [2004b]
1208	36°06′N	158°30′E	3346	PDW/LCDW	LR04	251	*Venti and Billups* [2012]
				Equatorial Pacific			
586	0°30′S	158°30′E	2218	PDW	LR04M&B	7	*Whitman and Berger* [1993]
806	0°19′N	159°22′E	2520	PDW	LR04	204	*Bickert et al.* [1997], *Karas et al.* [2009]
807	3°36′N	156°37′E	2804	PDW	LR04	168	*this study*
849	0°11′N	110°31′W	3851	PDW	LR04	210	*Mix et al.* [1995b]
V28-179	4°37′N	139°36′W	4509	PDW	LR04M	16	*Shackleton and Opdyke* [1977]
				South Pacific			
590	31°10′S	163°22′E	1293	AAIW	LR04M	5	*Elmstrom and Kennett* [1986], *Barton and Bloemendal* [1995]
209	15°56′S	152°11′E	1428	AAIW/PDW	LR04B	4	*Isern et al.* [1993]
1123	41°47´S	171°30′W	3290	LCDW	LR04	184	*Harris* [2002]
MV0502-4JC	50°20′S	148°08′W	4286	LCDW/AABW	Original	67	*Waddell et al.* [2009]
				South Atlantic			
1088	41°08′S	13°34′E	2082	UCDW	Original	78	*Hodell and Venz-Curtis* [2006]
704	46°53′S	7°25′E	2532	LCDW	LR04	195	*Hodell and Venz* [1992]
1090	42°55′S	8°54′E	3702	LCDW	LR04	156	*Venz and Hodell* [2002]
				Equatorial Atlantic			
999[c]	12°44′N	78°44′W	2828	AAIW/NADW	LR04	188	*Haug and Tiedemann* [1998]
925	4°12′N	43°29′W	3040	NADW	LR04	202	*Bickert et al.* [1997]
927	5°28′N	44°29′W	3326	NADW	LR04	188	*Bickert et al.* [1997]
929	5°59′N	43°44′W	4369	NADW/AABW	LR04	163	*Bickert et al.* [1997]
				North Atlantic			
982	57°31′N	15°53′W	1145	NADW	LR04	259	*Venz and Hodell* [2002]
552	56°03′N	23°13′W	2311	NADW	LR04M	102	*Shackleton and Hall* [1984], *Curry and Miller* [1989]
607	41°00′N	32°57′W	3427	NADW	LR04	174	*Raymo et al.* [1989]

[a]LR04 here stands for the oxygen isotope stratigraphy of *Lisiecki and Raymo* [2005], LR04M the magnetic polarity reversal ages of LR04, and LR04B the biochronology of Geological Time Scale 2012 [*Gradstein et al.*, 2012] rescaled to LR04. LR04M&B means both LR04M and LR04B are used. For Site 1148 the astronomically tuned age model of *Tian et al.* [2008] is used. For Site MV0502-4JC and 1088, the original age models from their references are used. See Text S3 and Tables S1 and S2 for the construction of age models.

[b]Number of benthic $\delta^{13}C$ data points between 2.4 and 1.7 Ma. Except Site 1208 which has five more data points for $\delta^{18}O$, all the other sites have the same number of $\delta^{13}C$ and $\delta^{18}O$ data points.

[c]These are marginal sea sites lying below the sill depths, but they are used to represent water masses at their sill depths and at the locations of the deep channels connecting the marginal basins to the open ocean. In all the section plots of this paper, a depth of 2400 m and a latitude of 19°27′N for South China Sea Sites 1143 and 1148 are used, which are the sill depth of Bashi Strait and the latitude of Site 1146 that lies close to the strait [*Wang and Li*, 2009]. For Site 999 in the Caribbean Sea, they are 1815 m and 17°30′N, determined by the Jungfern-Grappler Sill complex [*MacCready et al.*, 1999].

Cibicidoides are corrected by adding 0.64‰, and the $\delta^{13}C$ data are kept unchanged [*Shackleton and Hall*, 1984]. For ODP Site 1014, *Cibicidoides mckannai* was used but the original investigators carried out their own calibration, which is retained here (adding 0.2‰ to $\delta^{13}C$ and subtracting 0.09‰ from $\delta^{18}O$ to be equivalent to *C. wuellerstorfi*) [*Kwiek and Ravelo*, 1999]. A brief discussion of benthic $\delta^{13}C$ as a circulation tracer is presented in Text S2 [*Belanger et al.*, 1981; *Broecker and Maier-Reimer*, 1992; *Graham et al.*, 1981; *Lisiecki*, 2010; *Lynch-Stieglitz*, 2003; *Mackensen et al.*, 1993; *Schmittner et al.*, 2013; *Shackleton and Hall*, 1984; *Zahn et al.*, 1986]. In the following text, we will use benthic $\delta^{13}C$ and $\delta^{13}C_{DIC}$ interchangeably.

2.3. Age Models

The published age model of Site 807 was built on shipboard biostratigraphy, magnetostratigraphy, and planktonic foraminiferal oxygen isotope stratigraphy [*Jin et al.*, 2011; *Zhang et al.*, 2007]. We modify this model by tuning the early Pleistocene benthic $\delta^{18}O$ record to the LR04 Stack [*Lisiecki and Raymo*, 2005], using the automatic correlation technique developed by *Lisiecki and Lisiecki* [2002] (Figure S1 in the supporting

information). The time resolution of our record is ~3 ka, but there is a gap at marine isotope stage 89. Whenever possible, the age models of collected sites are tuned to the LR04 scale (Table 1). Many sites were used to construct the LR04 stack, and therefore, their LR04 age models already exist [*Lisiecki and Raymo*, 2005]. A few sites (Sites 209, 552, 586, 590, 1014, 1018, and V28-179) have very low resolutions that prohibit tuning based on oxygen isotope stratigraphy. We rescale their magnetic polarity reversal ages and bio-datum marker ages on the LR04 scale using a conversion table that links the LR04 scale to the Geology Time Scale 2012 (Table S1 in the supporting information) [*Gradstein et al*., 2012]. There are also three sites (Sites 1088, 1148, and MV0502-4JC) of intermediate resolution that we either retain the original age models or use the latest models available. See Text S3 for how these age models are constructed [*Gradstein et al*., 2012; *Hodell and Venz-Curtis*, 2006; *Lisiecki*, 2014; *Lisiecki and Raymo*, 2005; *Tian et al*., 2008, and references in Table 1]. Given the low temporal resolution of many sites, the discontinuity of benthic data after filtering out non-*Cibicidoides* data, possible mismatch during tuning, and sometimes weak glacial-interglacial variability (e.g., the long-term climate excursion dwarfed the glacial-interglacial variations at site MV0502-4JC), we will focus on the mean climate state instead of the glacial-interglacial variability in the studied interval.

2.4. A δ^{13}C-δ^{18}O Mixing Model

Benthic δ^{13}C is widely used as the sole mixing tracer in paleoceanography, under the assumption of "quasi-conservativeness" [*Bell et al*., 2015; *Hodell and Venz-Curtis*, 2006; *Lisiecki*, 2010; *Mix et al*., 1995b; *Raymo et al*., 1992, 1990, 1989, 2004; *Waddell et al*., 2009]. This approach is exemplified by the "%NCW" formulation developed by *Oppo and Fairbanks* [1987], in which case, the nonconservativeness of δ^{13}C due to remineralization is ignored and benthic δ^{13}C is interpreted on the ground of water mass mixing only, with the allowance of variable preformed end-member δ^{13}C. Alternatively, another approach acknowledges the remineralization effect but assumes that it is time invariant, as done in *Lisiecki* [2010]. However, given it is widely hypothesized that the distribution of the respired carbon pool in the deep ocean has changed in the past, dismissing the nonconservativeness of δ^{13}C or assuming it is constant might not be warranted.

The limitation of these approaches is due to the dependence of a nonconservative trace alone. Since the deepwater masses have at least two end-members, NADW and AABW, event under stringent constraint of mass conservation a conservative tracer must be used alongside with δ^{13}C in order to separate the mixing component from the remineralization effect, or multiple interrelated nonconservative tracers are required [*Gebbie and Huybers*, 2010; *Gebbie et al*., 2016; *Huybers et al*., 2007; *LeGrand and Wunsch*, 1995]. Benthic δ^{18}O would be the obvious choice of a conservative tracer, given both temperature and seawater δ^{18}O are conservative properties. This is rarely done in paleoceanography because unlike benthic δ^{13}C the benthic δ^{18}O of water mass end-members are usually indistinguishable. For example, in today's ocean NADW is saltier but warmer than AABW, two effects that largely cancel each other, leading to a rather small difference in benthic δ^{18}O. Similarly, on the δ^{13}C–δ^{18}O mixing space of *Duplessy et al*. [2002] Southern Ocean and North Atlantic deepwater masses cannot be separated by benthic δ^{18}O alone in the Last Glacial Maximum (LGM), and this small difference has made it difficult for models to distinguish the LGM circulation regime from the modern case [*Gebbie and Huybers*, 2006; *Marchal and Curry*, 2008].

The studied interval (2.4–1.7 Ma), in contrast, was a period the end-member difference was large enough that benthic δ^{18}O could be a useful tracer (Figure 3): the gradient of benthic δ^{18}O between the end-member sites chosen in this study, ODP 982 for NADW and MV0502-4JC for AABW, was ~1.3‰ in the studied interval but only ~0.4‰ in the LGM [*Venz and Hodell*, 2002; *Waddell et al*., 2009]. This difference is also much higher than the maximum interlaboratory offset of δ^{18}O (~0.4‰) reported in literature [*Hodell et al*., 2003b; *Ostermann and Curry*, 2000; *Zahn and Mix*, 1991].

To discuss the water mass mixing regime of this interval, we propose a two-tracer mixing model expressing the benthic δ^{13}C and δ^{18}O at a deepwater site as the linear combinations of these properties at two end-member sites representing NADW and AABW (Figure 3), plus interior sources:

$$\delta^{13}C_{site} = m_{NADW}\delta^{13}C_{NADW} + m_{AABW}\delta^{13}C_{AABW} - \delta^{13}C_{re}, \quad (1)$$

$$\delta^{18}O_{site} = m_{NADW}\delta^{18}O_{NADW} + m_{AABW}\delta^{18}O_{AABW}, \quad (2)$$

$$1 = m_{NADW} + m_{AABW}. \quad (3)$$

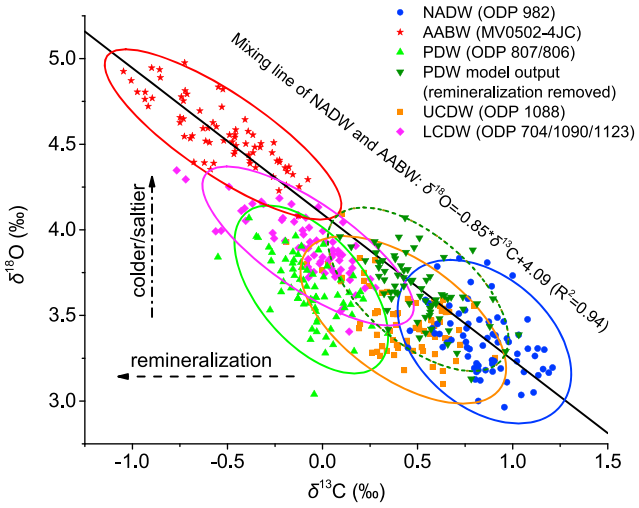

Figure 3. Water masses projected onto the benthic $\delta^{13}C$-$\delta^{18}O$ space for the 2.4–1.7 Ma interval. Following *Venz and Hodell* [2002], we choose Site 982 to represent NADW. We use MV0502-4JC to represent AABW as it is the deepest Southern Ocean site in our collection. For PDW, a stack of Sites 806 and 807 is used. Site 1088 is the only UCDW site, and Sites 704, 1090, and 1123 are also stacked together to represent LCDW. All the records are interpolated at 10 ka interval between 2.4 and 1.7 Ma before making the plot. The NADW-AABW mixing line is found by linear regression using the $\delta^{13}C$ and $\delta^{18}O$ data. The inverted dark green triangles represent the modeled PDW $\delta^{18}O$ and $\delta^{13}C$ data, calculated by using model output **m** and equations (1) and (2), but the remineralization term $\delta^{13}C_{re}$ has been subtracted from $\delta^{13}C$. Ellipses shown here are 95% confidence ellipses.

m_{NADW} and m_{AABW} are the mass fractions, and $\delta^{13}C_{re}$ is the remineralization term, or the interior source of $\delta^{13}C$, which has to be nonnegative (note the negative sign before it in equation (1)).Equation (2), which describes the conservativeness of benthic $\delta^{18}O$, can also be rewritten as three equations: one for the conservativeness of temperature (T), one for seawater $\delta^{18}O$ ($\delta^{18}O_{sw}$), and the third describing the dependence of benthic $\delta^{18}O$ on T and $\delta^{18}O_{sw}$, which is generally accepted to be a linear relationship [*Marchitto et al.*, 2014]. It is not necessary to deconvolve benthic $\delta^{18}O$ into temperature and $\delta^{18}O_{sw}$ components in the mixing model, as long as the calibration equation is linear [*Gebbie*, 2014; *Gebbie and Huybers*, 2006; *Marchal and Curry*, 2008]. By adding a relationship for benthic $\delta^{18}O$, the remineralization term can be separated from the mixing component of benthic $\delta^{13}C$ without making the aforementioned assumptions.

It is important to note the essential limitations of this model. First, it is valid when there are only two major mixing end-members. Modern water mass decomposition studies suggest that the Antarctic Intermediate Water (AAIW) also contributes considerably to global deepwater masses (13%–20%) [*DeVries and Primeau*, 2011; *Gebbie and Huybers*, 2010; *Khatiwala et al.*, 2012], but the lack of high-quality records precludes its inclusion in our model. Second, this model is applicable only when the isotopic properties of the end-members are sufficiently different.

Rearranging in vector forms, let

$$\mathbf{y} = \begin{bmatrix} \delta^{13}C_{site} \\ \delta^{18}O_{site} \\ 1 \end{bmatrix}; \ \mathbf{m} = \begin{bmatrix} m_{NADW} \\ m_{AABW} \\ \delta^{13}C_{re} \end{bmatrix}, \tag{4}$$

and rewrite equations (1–3) in the canonical form [*Wunsch*, 2006],

$$\mathbf{y} = \mathbf{Em} + \mathbf{n}, \tag{5}$$

where **E** is a 3×3 full rank matrix (if $\delta^{18}O_{NADW} \neq \delta^{18}O_{AABW}$) given by

$$\mathbf{E} = \begin{bmatrix} \delta^{13}C_{NADW} & \delta^{13}C_{AABW} & -1 \\ \delta^{18}O_{NADW} & \delta^{18}O_{AABW} & 0 \\ 1 & 1 & 0 \end{bmatrix}, \tag{6}$$

and **n** is the noise term. Models like this have been widely used in water mass decomposition studies [e.g., *Poole and Tomczak*, 1999], and more sophisticated inversion techniques have been used for ocean state

estimates of the LGM [*Gebbie*, 2012, 2014; *LeGrand and Wunsch*, 1995; *Marchal and Curry*, 2008]. To get **m**, we solve the nonnegative and weighted linear least squares problem by minimizing the objective function

$$J = \mathbf{n}^T\mathbf{W}\mathbf{n},\ \mathbf{m} \geq \mathbf{0}, \tag{7}$$

where **W** is the weighting matrix, usually constructed as a diagonal matrix having the reciprocals of squared observational errors corresponding to the row elements in **y** [*de Brauwere et al*., 2007; *Gebbie and Huybers*, 2010]. However, unlike temperature and salinity, the analytical errors of benthic δ^{13}C and δ^{18}O are not useful weights because duplicate measurements generally yield greater uncertainties, especially when there are only one or two specimens analyzed. Interlaboratory offsets, particularly for δ^{18}O, are also usually much larger than reported analytical precisions [*Hodell et al*., 2003b; *Ostermann and Curry*, 2000; *Zahn and Mix*, 1991]. Instead, we use min(std($\delta^{13}C_{NADW\text{ - site}}$), std($\delta^{13}C_{AABW\text{ - site}}$))^2 and min(std($\delta^{18}O_{NADW\text{ - site}}$), std($\delta^{18}O_{AABW\text{ - site}}$))^2 as the weights for δ^{13}C and δ^{18}O, respectively, for each site: we first compute the time-dependent gradients in the studied interval between the targeted site and the two end-members and then find the standard deviations of these two gradients in the studied interval and use the smaller one. They are chosen to lessen the constraints that δ^{13}C and/or δ^{18}O would otherwise impose on the solution when one of them is too close to the end-member values. The mass conservation equation should be strictly satisfied, but giving it too much weight would diminish the capacities of δ^{13}C and δ^{18}O as circulation tracers. We choose to set its weight to be 10 times of the weight of δ^{13}C or δ^{18}O, whichever is greater.

3. Results and Discussion

3.1. Vertical Structures of δ^{13}C Between 2.4 and 1.7 Ma

A brief description of modern deepwater circulation using $\delta^{13}C_{DIC}$ and salinity distributions (Figure 2) is included in Text S4 [*Bostock et al*., 2010; *Emile-Geay et al*., 2003; *Kawabe and Fujio*, 2010; *Key et al*., 2004; *Rintoul et al*., 2001; *Schmittner et al*., 2013; *Talley*, 2013; *Talley et al*., 2011; *Warren*, 1983]. We begin our discussion with the mapping of deepwater masses using benthic δ^{13}C profiles. Since we are only interested in the mean climate state, we take the average values of benthic δ^{13}C records in the studied interval while reporting the glacial-interglacial variability as standard deviations (Table S3). Individual records are plotted in Figures S2 and S3.

3.1.1. South Pacific and South Atlantic

The Southern Ocean connects the circulation branches in the Atlantic and Pacific today so it merits to be discussed first. Vertical profiles of δ^{13}C in the South Pacific and South Atlantic between 40°S and 50°S were very similar during the studied interval, suggesting that the Southern Ocean water masses were well connected in these two basins (Figure 4). AAIW, represented by the Deep Sea Drilling Program Sites 209 and 590, was where the vertical δ^{13}C maximum resided in the South Pacific like it does today (Figures 2b and 3). In contrast, below 2000 m the water column structure was sharply different. In the modern South Pacific, the vertical δ^{13}C minimum of the Upper Circumpolar Deep Water (UCDW) lies at ~2000 m around 40°S and beneath that δ^{13}C increases slightly toward the bottom with an almost indistinguishable maximum at ~3200 m, corresponding to the salinity maximum of the Lower CDW (LCDW) (Figures 2b and 3). In the modern South Atlantic, the δ^{13}C minimum of UCDW is shallower (~1500 m), and the intrusion of NADW creates a δ^{13}C maximum at ~2500 m (Figure 2c). Site 1088 from the South Atlantic is placed midway between these two extrema, and its δ^{13}C is higher than that at the same depth in the Pacific today. Yet in the studied interval, this site fits closely into the South Pacific profile (Figure 4). Also, there is little δ^{13}C gradient between Sites 1088 and 1090 today (Figure 2b), as confirmed by the compilation of Holocene *C. wuellerstorfi* data [*Hodell et al*., 2003a]. On the contrary, deep sites below ~3500 m in both basins were much more ^{13}C-depleted between 2.4 and 1.7 Ma, and the δ^{13}C of the bottommost site, MV0502-4JC, reached as low as −1.1‰. Sites 704 and 1090 were bathed in the same water mass, and they had similar δ^{13}C values, implying the modern-like outcrop of iso-surfaces existed during the studied interval [*Hodell and Venz-Curtis*, 2006]. In summary, the vertical δ^{13}C structures suggest that the deep Southern Ocean was well connected but stratified in both the Pacific and Atlantic sectors in the studied interval.

3.1.2. Equatorial and North Pacific

We combine sites from the Equatorial and North Pacific to create a single vertical profile of δ^{13}C in the studied interval (Figure 4). Today, the major difference between these two latitude bands lies above 2000 m, where

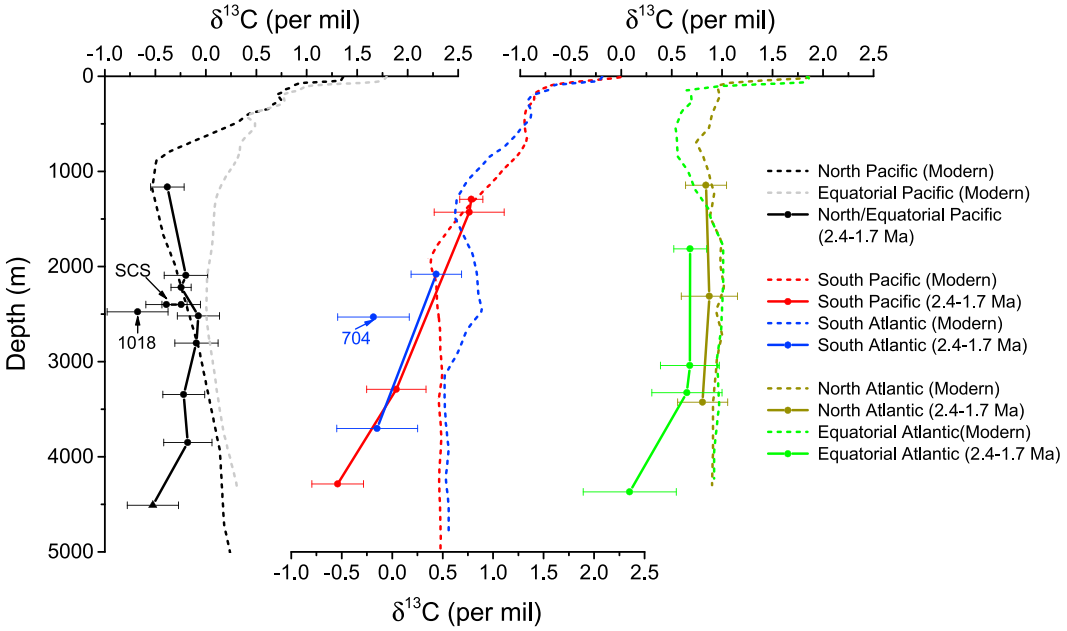

Figure 4. Vertical profiles of averaged benthic $\delta^{13}C$ values in the deep ocean between 2.4 and 1.7 Ma compared with today. Data used to create this figure are reported in Table S3. Modern data are from *Schmittner et al.* [2013], and the locations of modern profiles are indicated in Figure 2 (black filled squares in Figure 2a and purple dash lines in Figures 2b and 2c). Error bars represent standard deviations, which reflect mostly glacial-interglacial variability. Site 1018 is not used in creating the vertical profile because we deem its anomalously low value reflected local imprint rather than water mass signal. See discussion in section 3.1.2. Sites 1143 and 1148 from the South China Sea are also not included in the profile as they lie beneath the sill depth. Site 704, because of the outcrop of the Southern Ocean water masses near Antarctica, is bathed in the same water mass as Site 1090 today despite it is much shallower. This seems to be also the case in the studied interval, and therefore, it is not plotted on the vertical profile.

the North Pacific values are much more negative because of stronger remineralization effect, but below that depth divergence is small (Figures 2b and 4). The profile in the studied interval follows the modern pattern closely up to 3000 m, below which it converges to the negative Southern Ocean values (Figure 4). In the modern Equatorial and North Pacific, $\delta^{13}C$ increases toward the bottom because AABW transports high $\delta^{13}C$ water mass northward (Figure 2b). In contrast, in the studied interval the case was this Southern Ocean source water was even more ^{13}C-depleted than PDW (Figure 4).

The only anomaly above 3000 m is Site 1018 from the eastern North Pacific (Figure 4), the $\delta^{13}C$ of which (−0.68‰) was much lower than the western sites at similar depth (2500 m) in the studied interval. This extreme negative value at Site 1018, when compared with Sites 1014 and 849 also from the eastern North Pacific, prompted *Kwiek and Ravelo* [1999] to conclude the $\delta^{13}C$ minimum in the North Pacific deepened to 2500 m (~1500 m nowadays; Figure 2b) after 2.7 Ma, and they hypothesized that this was due to the enhancement of the North Pacific Intermediate Water (NPIW). However, our compilation does not support this hypothesis in the studied interval (Figure 4). Sites 1146, 586, and 806 from the western North Pacific between 2000 and 2500 m had $\delta^{13}C$ values in the studied interval similar to today. Sites 1148 and 1143 from the SCS are not used to create the profile in Figure 4 because they lie beneath the sill depth (2400 m), and their slightly lower $\delta^{13}C$ values probably reflect longer resident time and stronger remineralization effect in the marginal sea. But even these sites have much higher $\delta^{13}C$ than Site 1018. Considering the significant zonal and meridional nutrient gradients in the North Pacific today [*Talley et al.*, 2011], Site 1018 is expected to have lower $\delta^{13}C$ when compared to these sites to the southwest. But can this lead to an ~0.6‰ gradient? Existing $\delta^{13}C_{DIC}$ data are too sparse to fully resolve this issue, but we find from the compilation of *Schmittner et al.* [2013] that the modern $\delta^{13}C_{DIC}$ difference at ~2500 m is only ~0.2‰ between one hydrographic station (164.91°E, 0.02°N), that is close to Sites 586 and 806, and the other (127.61°W, 42.13°N) that is near Site 1018 (Figures S4a and 4b). Further, using the apparent oxygen utilization (AOU) data from the Global Data Analysis

Project (GLODAP) [*Key et al*., 2004] (which has much better spatial coverage) and the AOU-$\delta^{13}C_{DIC}$ relationship (0.0075‰/μmol · kg^{-1}) from *Kroopnick* [1985], we find an alternative estimate, ~0.25‰, for the modern $\delta^{13}C_{DIC}$ difference between these two locations (Figure S4c). It appears to explain the negative $\delta^{13}C$ value at Site 1018 in the studied interval, not; we need to invoke stronger zonal and/or meridional gradients in the North Pacific, which, however, did not manifest at Sites 1014 and 849 (Figure 4). Thus, we suggest in the studied interval the $\delta^{13}C$ of Site 1018 was probably controlled by local factors rather than background water mass property, and the inference of NPIW enhancement is likely not true. Better ventilation of the intermediate water should have resulted in higher-than-today $\delta^{13}C$ at Site 1014, but this is not seen (Figure 4). The original investigators corrected the *C. mckannai* $\delta^{13}C$ data of Site 1014 by adding 0.2‰ [*Kwiek and Ravelo*, 1999], and without this correction its $\delta^{13}C$ in the studied interval would only be lower (though still falls on the modern profile). More importantly, studies from Site 882 (50°21′N, 167°35′E) have presented compelling evidence asserting the onset of modern style stratification in the subarctic North Pacific after 2.7 Ma [e.g., *Haug et al*., 1999; *Swann*, 2010], rendering the argument of NPIW enhancement in the studied interval unlikely. Hence, we conclude that the vertical water mass structure above 3000 m in the North Pacific between 2.4 and 1.7 Ma was similar to today.

3.1.3. Equatorial and North Atlantic

NADW in the Equatorial and North Atlantic today is characterized by an almost uniformly distributed $\delta^{13}C$ of ~1.0‰ (Figure 2c). There is little difference between these two latitude bands, and only south of the equator the intrusion of AABW at depth becomes noticeable. In the studied interval, $\delta^{13}C$ was also vertically uniform at these two places above 3500 m (Figure 4), but near the equator below this depth the $\delta^{13}C$ of Site 929 deviated toward the Southern Ocean values as seen in the deep Pacific. Unlike in the Pacific and the Southern Ocean, sites in the North and Equatorial Atlantic generally had stronger glacial-interglacial variability between 2.4 and 1.7 Ma (Figure 4). The interglacial $\delta^{13}C$ values of these sites above 3500 m clustered around 1.0‰, while in the glacial maxima deeper sites like Sites 929 and 927 sometimes excursed strongly toward lower $\delta^{13}C$ values, previous explained as the result of the intrusion of Southern Ocean water mass [*Bickert et al*., 1997; *Venz and Hodell*, 2002].

3.2. End-Members of Water Mass Mixing

The $\delta^{13}C$ of PDW is lower than both NADW and AABW today, reflecting its older age (Figure 2) [*Schmittner et al*., 2013]. However, in the 2.4–1.7 Ma interval, it was not PDW but AABW that had the lowest $\delta^{13}C$ (Figure 4). Does this imply a different mixing regime? As the vertical structure of $\delta^{13}C$ in the North Pacific above 3000 m was similar to today (Figure 4), there is no evidence of deepwater formation or intermediate water enhancement in the studied interval. Therefore, it is reasonable to assume that deepwater formation sites also lay in the North Atlantic and the Southern Ocean back then.

A benthic $\delta^{13}C$-$\delta^{18}O$ plot is used to identify end-members of water mass mixing (Figure 3) [*Duplessy et al*., 2002]. The plot suggests the two-end-member, namely, NADW-AABW, mixing regime existed between 2.4 and 1.7 Ma, and PDW, UCDW, and LCDW all fall left to the mixing line as required by the remineralization effect on $\delta^{13}C$. However, the preformed properties of the end-members were very different from today. While the $\delta^{13}C$ of NADW clustered around its modern value (~1‰), the $\delta^{13}C$ of AABW was on average ~1‰ lower than today (Figures 2–4). On the other hand, the benthic $\delta^{18}O$ of AABW was ~1.3‰ higher than NADW. Figure 3 also gives us confidence that the choice of MV0502-4JC as the AABW representative is reasonable. It shows organized relationship among water masses, suggesting the rather "anomalously" high $\delta^{18}O$ and low $\delta^{13}C$ of MV0502-4JC are not localized features. Further, another site, ELT 25-11, from the same latitude and similar depth in the Pacific sector of the Southern Ocean, revealed similar evolution of benthic $\delta^{18}O$ and $\delta^{13}C$ during the Plio-Pleistocene transition despite being 20° to the east [*Waddell et al*., 2009]. It is not included in our collection because of poor recovery, but such evidence suggests that our end-member choice is not biased by local hydrological factors.

The strong differences of benthic $\delta^{13}C$ and $\delta^{18}O$ between NADW and AABW make it possible to employ the $\delta^{13}C$-$\delta^{18}O$ mixing model described in section 2.4. We first apply this model to unravel the composition of PDW represented by Site 807/806 in the studied interval (Figure S5). Benthic records of each water mass are linearly interpolated at 10 ka intervals between 2.4 and 1.7 Ma, and we calculate the water mass fractions and the remineralization term at each time point. The problem is solved by using the nonnegative linear least squares routine of MATLAB. Modeled benthic $\delta^{13}C$ and $\delta^{18}O$ of PDW fit the observations very closely

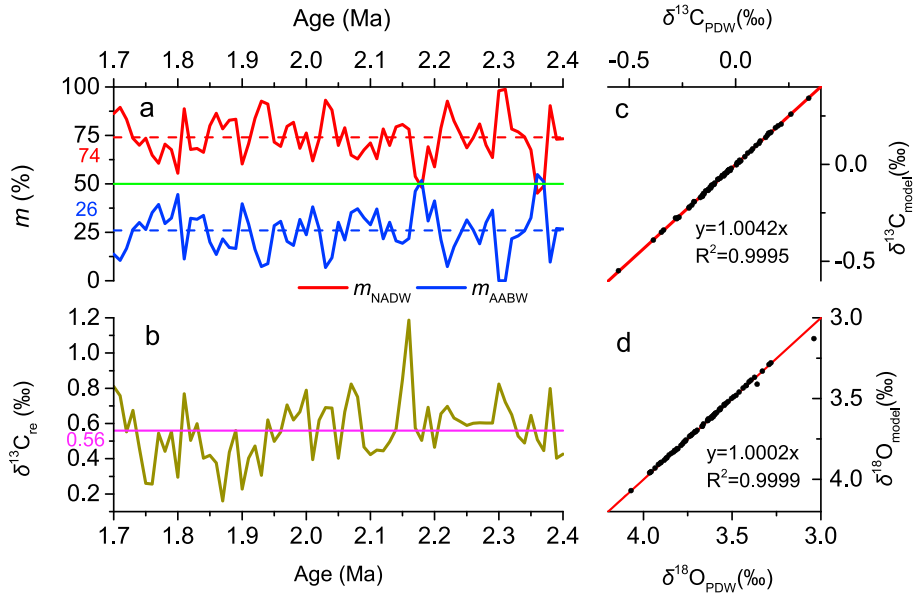

Figure 5. Results of the $\delta^{13}C$-$\delta^{18}O$ mixing model for PDW. Benthic records used in the model follows the description in Figure 3. (a) Model results of m_{NADW} and m_{AABW}. The average values of m_{NADW} (red dash) and m_{AABW} (blue dash) as well as the equal mixing ratio line (green solid) are also plotted. (b) Model result of $\delta^{13}C_{re}$ (dark yellow solid line) and its average (magenta solid). (c) Comparison of model result $\delta^{13}C_{model}$ calculated by using equation (1) with the original PDW record $\delta^{13}C_{PDW}$. (d) Comparison of model result $\delta^{18}O_{model}$ calculated by using equation (2) with the original PDW record $\delta^{18}O_{PDW}$. The two regression lines in Figures 5c and 5d are found by setting the intercepts to zero.

(Figures 5c and 5d). The $\delta^{13}C_{re}$ of PDW also falls within a reasonable range (0.56 ± 0.17‰; Figure 5b), close to the value (0.5‰) estimated by *Lisiecki* [2010] for the past 800 ka. Most interestingly, m_{NADW} (74 ± 11%) was consistently much higher than m_{AABW} (26 ± 12%).

Modern water mass decomposition studies show that the deep water between 2000 and 3000 m in the North Pacific is made of ~10%–25% NADW, ~50%–60% AABW, ~15%–20% AAIW with the rest coming from NPIW and surface sources [*DeVries and Primeau*, 2011; *Gebbie and Huybers*, 2010; *Johnson*, 2008; *Khatiwala et al.*, 2012]. Comparing with today, NADW in the 2.4–1.7 Ma interval contributed a much greater portion to PDW at the expense of AABW, suggesting a different circulation pattern. Because the records of AAIW and other intermediate and surface water masses are currently either lacking or fragmentary in the early Pleistocene, they are not represented in the mixing model though we acknowledge that they might be considerable sources for PDW too. In fact, our results suggest the mixing between NADW and AABW alone could count for most of the variability in the benthic records of PDW.

In this model, we do not account for the measurement uncertainty due to interlaboratory offsets, which could be an issue for benthic $\delta^{18}O$ [*Hodell et al.*, 2003b; *Ostermann and Curry*, 2000; *Zahn and Mix*, 1991]. However, simple sensitivity analyses can be made to evaluate the effect of this uncertainty. If we subtract 2‰ uniformly from the benthic $\delta^{18}O$ record of AABW and keep all the other records the same, m_{NADW} will decrease to 68 ± 14% for PDW. If we add 2‰ instead, m_{NADW} will increase to 78 ± 10% for PDW. Only under rather extreme scenarios, such as subtracting >4‰ from the benthic $\delta^{18}O$ record of AABW would m_{NADW} of PDW be significantly lower than 50% in the studied interval. Therefore, our conclusion is robust within reasonable estimates of such offsets.

3.3. Circulation Regime

We further apply this model to the high-resolution sites in our collection and use the mean values of m_{NADW} and $\delta^{13}C_{re}$ between 2.4 and 1.7 Ma to trace the circulation pathway (Figure 6 and Table S4). Some features are well constrained despite limited spatial coverage. Water mass compositions of the North Pacific and North

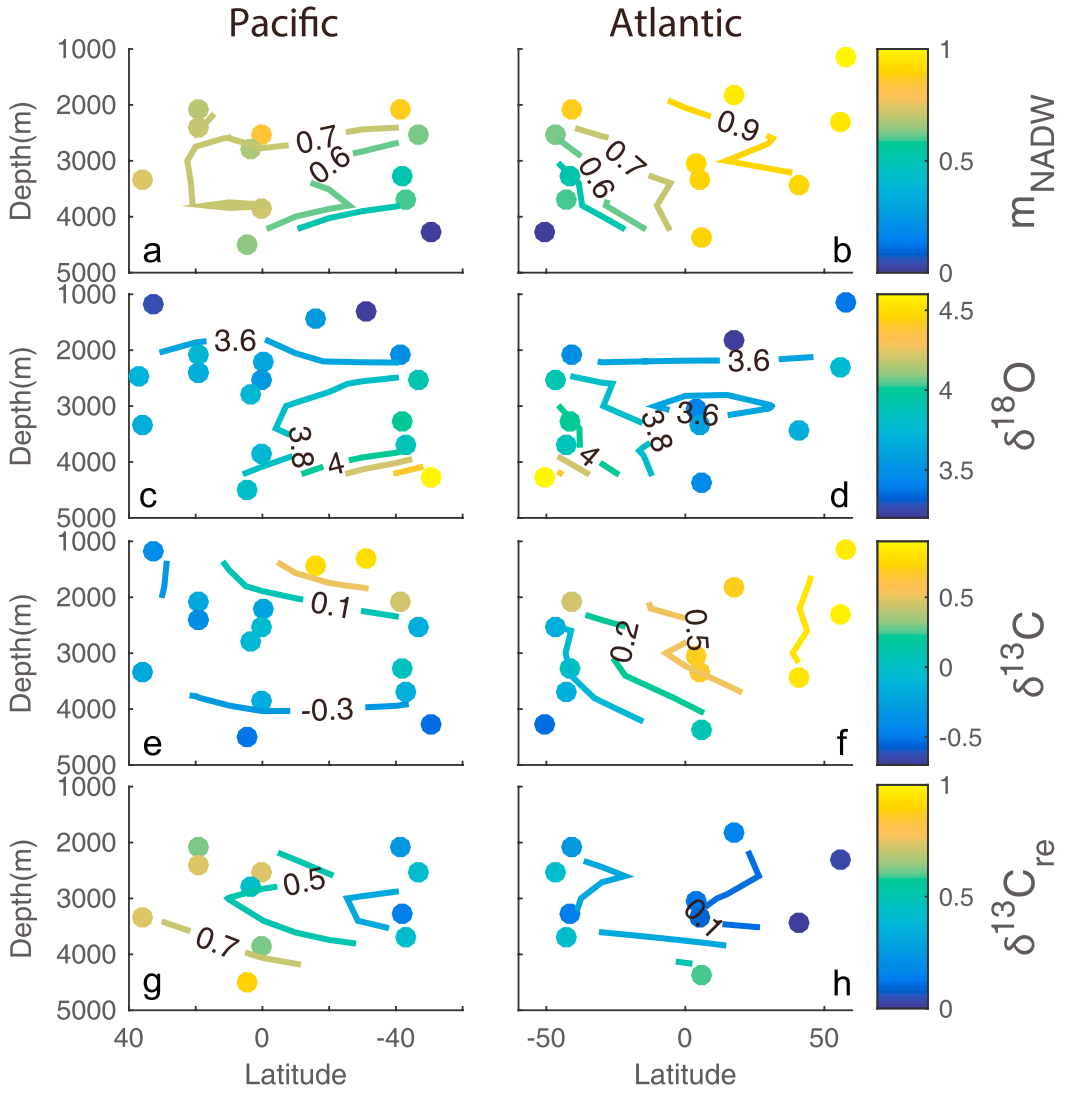

Figure 6. Distributions of (a and b) m_{NADW}, (c and d) benthic $\delta^{18}O$, (e and f) benthic $\delta^{13}C$, and (g and h) $\delta^{13}C_{re}$ in the Pacific and Atlantic in the 2.4–1.7 Ma interval. m_{NADW} and $\delta^{13}C_{re}$ distributions are created by using model results of high-resolution sites listed and reported in Table S4. Note that Sites 982 and MV0502-4JC are not plotted in Figures 6g and 6h as they are taken as end-members. Benthic $\delta^{18}O$ distribution is created by using all the sites and the original $\delta^{18}O$ data listed in Table S3. Benthic $\delta^{13}C$ distribution is created by using all but Site 1018 in Table S3, because of its anomalous behavior discussed in section 3.1.2. The Southern Ocean sites are plotted on both the Pacific and Atlantic sections. Contours are created based on natural neighbor interpolation (10° × 400 m in the Pacific and 15° × 400 in the Atlantic, and no extrapolation is done), and they are only meant to help identify large-scale features.

Atlantic were rather homogeneous (Figures 6a and 6b). More importantly, like the Atlantic Ocean, the Pacific was also ventilated primarily by NADW (~70% on average), while AABW was mostly confined to the deep Southern Ocean as well as the bottom of the other basins (Figures 6a and 6b). Stratification of the Southern Ocean deepwater masses is further confirmed by the distributions of m_{NADW} and $\delta^{13}C_{re}$, as well as benthic $\delta^{13}C$ and $\delta^{18}O$ (Figure 6). $\delta^{13}C_{re}$ shows progressively increasing remineralization effect from the North Atlantic to the Southern Ocean and then to the North Pacific, consistent with the general "aging" pattern of deepwater masses today (Figures 2b and 2c). Interestingly, the greatest remineralization effect in the studied interval was found at the bottom instead of middepth in the Pacific as today (Figure 2b), likely reflecting storage of respired carbon in the bottom water.

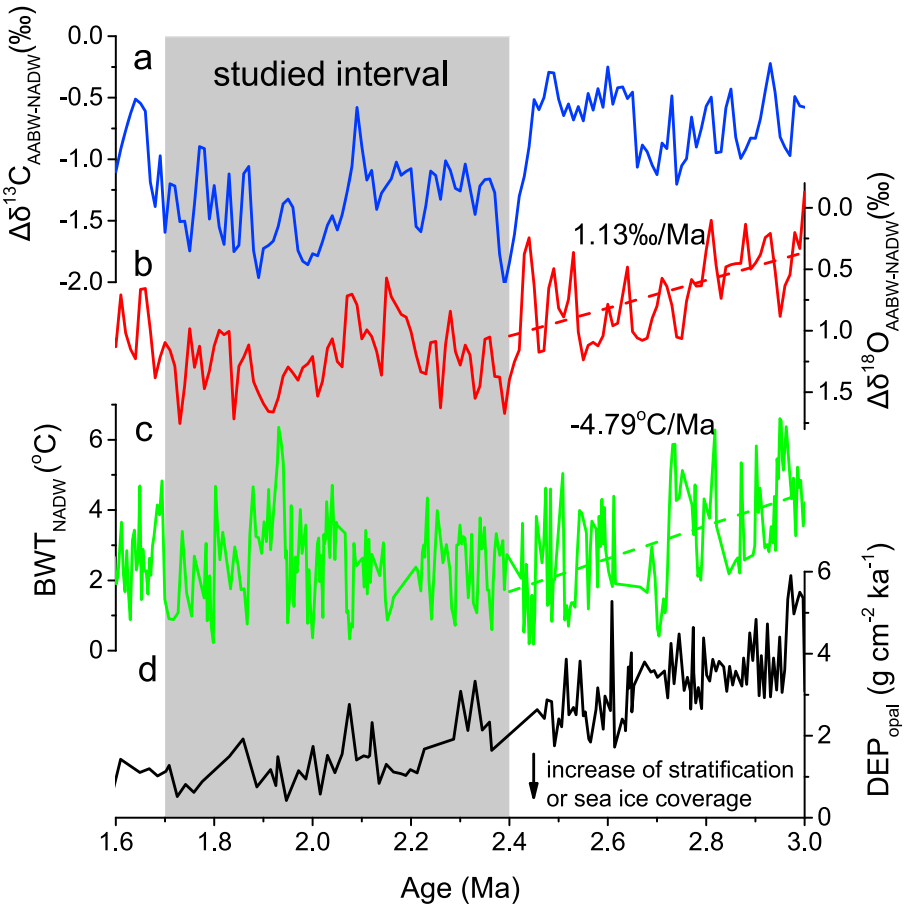

Figure 7. The initiation of the circulation pattern in the 2.4–1.7 Ma interval and its relation to the onset of NHG. (a) The $\delta^{13}C$ gradient between AABW (Site MV0502-4JC) and NADW (Site 982). (b) The $\delta^{18}O$ gradient between AABW and NADW. (c) the BWT record of NADW (Site 607). The age model of this record was also tuned to the LR04 stack by its original authors [*Sosdian and Rosenthal*, 2009]. The dashed lines in Figures 7b and 7c are linear regression lines calculated by using the data between 3.0 and 2.4 Ma. Labeled numbers are the slopes. (d) Opal depositional rate from Site 1096 in the Southern Ocean [*Hillenbrand and Fütterer*, 2001; *Hillenbrand and Ehrmann*, 2005]. The original age model of Site 1096 was based on magnetostratigraphy, and we use the LR04 magnetic reversal ages to update this model to make it compatible to other sites.

3.4. Connection to the Onset of Northern Hemisphere Glaciation

3.4.1. Initiation of the Circulation Regime Between 2.4 and 1.7 Ma

To understand how such a circulation pattern between 2.4 and 1.7 Ma was initiated, we compare the AABW-NADW (MV0502-4JC-Site 982) benthic isotope gradients $\Delta\delta^{13}C_{AABW\text{-}NADW}$ and $\Delta\delta^{18}O_{AABW\text{-}NADW}$, and the BWT record (Site 607) of NADW from 3.0 to 1.6 Ma (Figure 7). The behaviors of these three proxies were very different. While the BWT of NADW and $\Delta\delta^{18}O_{AABW\text{-}NADW}$ were marked by gradual changes from 3.0 to 2.4 Ma, $\Delta\delta^{13}C_{AABW\text{-}NADW}$ seems to remain nearly constant until it crossed a certain threshold just before 2.4 Ma. The increase of $\Delta\delta^{18}O_{AABW\text{-}NADW}$ from 3.0 to 2.4 Ma suggests either a decrease of AABW-NADW BWT gradient or an increase of AABW-NADW salinity gradient related to $\delta^{18}O_{sw}$, or a combination of both. Using a relation between benthic $\delta^{18}O$, $\delta^{18}O_{sw}$ and BWT we can quantify the relative contributions of these two factors:

$$\delta^{18}O - \delta^{18}O_{sw} + 0.27 = -0.224BWT + 3.53, \tag{8}$$

in which $\delta^{18}O$ is on the PDB standard and $\delta^{18}O_{sw}$ is on the SMOW standard [*Marchitto et al.*, 2014]. According to this equation, we infer that the rate change of $\Delta\delta^{18}O_{AABW\text{-}NADW}$ can be expresses as

$$\frac{d}{dt}\Delta\delta^{18}O_{AABW\text{-}NADW} = \frac{d\delta^{18}O_{sw}}{dS} \times \frac{d}{dt}\Delta S_{AABW\text{-}NADW} - 0.224\left(\frac{d}{dt}BWT_{AABW} - \frac{d}{dt}BWT_{NADW}\right), \tag{9}$$

the first and the second terms on the right-hand side of the equation represent the contributions of the AABW-NADW salinity (a $\delta^{18}O_{sw}$-salinity relation is incorporated) and BWT gradients to the benthic $\delta^{18}O$ gradient respectively.

The $\frac{d}{dt}\Delta\delta^{18}O_{AABW\text{-}NADW}$ is estimated by using the linear regression slope of $\Delta\delta^{18}O_{AABW\text{-}NADW}$ versus time between 3.0 and 2.4 Ma, and the result is 1.13‰/Ma (Figure 7b). The average change of $\Delta\delta^{18}O_{AABW\text{-}NADW}$ for this 0.6 Ma interval was therefore 0.67‰. The $\frac{d}{dt}BWT_{NADW}$ is also approached by the linear regression slope (BWT_{NADW} versus time), assuming that Site 607 is representative of NADW and its BWT history was similar to Site 982, and the result is −4.79°C/Ma (Figure 7c) between 3.0 and 2.4 Ma. There is no BWT record for any Southern Ocean sites in the 3.0–2.4 Ma interval, but the Pliocene Research, Interpretation and Synoptic Mapping-3D (PRISM-3D) project provided BWT reconstructions for several Southern Ocean sites for the 3.29–2.97 Ma interval (the PRISM interval, considered to be warmer than today) [*Dowsett et al.*, 2009], which can serve as the upper bound of the BWT of AABW at 3.0 Ma. According to the PRISM-3D result, BWT at Sites 1123 and 1090 was 2.7°C and 2.0°C, respectively, in the PRISM interval. Considering that the AABW end-member Site MV0502-4JC is deeper, its temperature is more likely lower than 2.0°C at 3.0 Ma. After 3.0 Ma the temperature history at Site MV0502-4JC can only be hypothesized because of the lack of any direct or indirect data, but a BWT increase should be rejected for it would require too great a salinity gradient increase to account for the rise of $\Delta\delta^{18}O_{AABW\text{-}NADW}$, and it would also contradict the general notion of the cooling trend during the Plio-Pleistocene transition [*Fedorov et al.*, 2013]. On the other hand, it is also unlikely that the BWT minimum at this site between 3.0 and 2.4 Ma can be lower than during the LGM, given that the highest benthic $\delta^{18}O$ in the Plio-Pleistocene transition did not exceed that of the LGM at this site [*Waddell et al.*, 2009]. By separating the salinity effect from benthic $\delta^{18}O$ using pore water $\delta^{18}O$ and chlorinity, the BWT at Southern Ocean Sites 1123 and 1093 (5°51.935′E, 49°58.588′S, 3626 m) was reconstructed to be −1.2°C and −1.3°C in the LGM, respectively [*Adkins et al.*, 2002]. Benthic Mg/Ca indicated that the BWT at Site 1123 was in the range of −1.5 to −2°C in glacial maxima after 1.6 Ma [*Elderfield et al.*, 2012]. These data provide a constraint that the change of BWT at AABW Site MV0502-4JC from 3.0 to 2.4 Ma was unlikely more severe (in the absolute value) than −4°C (from +2°C to −2°C), and therefore, the rate change of BWT, $\frac{d}{dt}BWT_{AABW}$, was unlikely greater than −6.67°C /Ma in this 0.6 Ma interval.

Using these estimates, we find that the contribution of AABW-NADW BWT gradient change (second term in equation (9)) to the 0.67‰ $\Delta\delta^{18}O_{AABW\text{-}NADW}$ increase from 3.0 to 2.4 Ma was 0.25‰; thus, the rest 0.42‰ must be attributed to an increase of AABW-NADW salinity gradient (first term in equation (1)). To convert this number to a salinity gradient, i.e., $\Delta S_{AABW\text{-}NADW}$ in equation (9), we assume that the $\delta^{18}O_{sw}$-salinity relationship was similar to today and we use a range of values, i.e., 0.23–0.51‰ per salinity unit for $\frac{d\delta^{18}O_{sw}}{dS}$, to accommodate the difference of this relationship between AABW and NADW in today's ocean [*LeGrande and Schmidt*, 2006]. Under these assumptions, we estimate that the salinity of AABW increased 0.8 to 1.8 unit relative to NADW from 3.0 Ma to 2.4 Ma, which is likely a lower limit because of the temperature estimates used. We point out that we can only estimate the change of salinity gradient from 3.0 to 2.4 Ma rather than the absolute value of the gradient at any particular point. Given that at ~3.0 Ma $\Delta\delta^{18}O_{AABW\text{-}NADW}$ was near 0‰, and assuming the BWT of NADW was higher than AABW, it is then expected that NADW had slightly higher salinity at ~3.0 Ma (today, this difference is ~0.4 [*Talley et al.*, 2011]). However, this 0.8–1.8 unit increase of $\Delta S_{AABW\text{-}NADWW}$ from 3.0 to 2.4 Ma would probably have reversed the pre-3.0 Ma salinity gradient and made AABW much saltier and therefore denser than NADW by 2.4 Ma, resulting in Southern Ocean deep stratification in the 2.4–1.7 Ma interval (Figures 4 and 6). This salinity gradient reversal, we hypothesize, was responsible for the reduction of the volume of the ocean ventilated by AABW and the negative excursion of its $\delta^{13}C$ (Figures 4 and 6).

Although our estimates suggest the direct contribution of temperature change to the water mass reorganization from 3.0 to 2.4 Ma and eventually the circulation pattern reconstructed between 2.4 and 1.7 Ma was relatively small, its effect might have been amplified by positive feedback. Discussing the origin of the extremely cold and salty AABW in the LGM, *Adkins* [2013] hypothesized that the temperature decrease of NADW and the resulting reduction of southward heat transport could lead to less sea ice melting around the

continental shelf of the Antarctica, and therefore increase the salinity of AABW. This idea explicitly linked the development of stratification to sea ice expansion, and evidence suggests that such a mechanism was also at play during the Plio-Pleistocene transition. Diatom assemblage and other proxies from the Antarctic Drilling Program's AND-1B core recovered beneath the Ross Ice Shelf demonstrated the expansion of polar ice sheet at ~3 Ma and subsequent increase of sea ice extend/duration at ~2.6 Ma [*McKay et al*., 2012]. The decline of opal depositional rate from 3.0 to 2.4 Ma at Sites 1095 and 1096 next to the Atlantic Peninsula was also suggested to indicate the development of Antarctic stratification and sea ice growth (Figure 7d) [*Hillenbrand and Fütterer*, 2001; *Hillenbrand and Ehrmann*, 2005; *Sigman et al*., 2004]. Consistent with this hypothesis, it was found from 3.0 to 2.5 Ma, the deep ocean heat transport from the North Atlantic to the Pacific increased at the expense of the Southern Ocean, and synchronously the ventilation of the deep Pacific by NADW became increasingly important [*Woodard et al*., 2014], agreeing with our reconstruction between 2.4 and 1.7 Ma.

3.4.2. Implication for the Global Carbon Cycle

The global carbon cycle is widely implicated as a main factor driving the onset of NHG [*Bell et al*., 2015; *Hodell and Venz-Curtis*, 2006; *Waddell et al*., 2009], particularly in light of the concurrent decrease of atmospheric CO_2 [*Bartoli et al*., 2011; *Martinez-Boti et al*., 2015]. It is generally hypothesized that increasing carbon storage in the deep ocean was partially responsible for the cooling trend during the Plio-Pleistocene transition and the onset of NHG [*Hodell and Venz-Curtis*, 2006; *Waddell et al*., 2009], but separating the remineralization component of benthic $\delta^{13}C$, the one that actually measures deep carbon storage, from the mixing component has not been done before. Our mixing model makes this separation possible.

The model reveals two important aspects of the deep ocean carbon pool in the studied interval. First, the preformed $\delta^{13}C$ of AABW was much lower than today (Figures 4 and 6). This has been widely discussed in previous studies and was interpreted to be the result of either reduced air-sea gas exchange due to sea ice expansion or storage of respired carbon in this water mass or a combination of both [*Hodell and Venz-Curtis*, 2006; *Waddell et al*., 2009]. Better understanding of the surface water property around the Antarctica can help differentiate the effect of gas exchange from that of carbon accumulation. This is not attempted in this study, and it is certainly reasonable to believe that both factors were at play. A more critical result, however, is that the observed low $\delta^{13}C$ in the deep (>4000 m) Pacific and Atlantic between 2.4 and 1.7 Ma (Figure 4) was primarily the consequence of remineralization effect ($\delta^{13}C_{re}$), rather than simply mixing with the ^{13}C-depleted AABW (Figure 6 and Table S4). This implies that the presence of negative benthic $\delta^{13}C$ at deep Pacific and Atlantic is not necessarily indicative of greater AABW intrusion but could rather reveal carbon accumulation. It is important to clarify that this remineralization effect was superimposed on whatever remineralization effect that was already present in the water mass end-members, and it constrains the carbon pool that was in addition to the preformed pool. Thus, regardless how AABW acquired its negative preformed $\delta^{13}C$, our reconstruction of $\delta^{13}C_{re}$ directly supports the existence of a respired carbon pool sitting on the seafloor in this post-NHG interval (Figure 6).

We further hypothesize that the presence of this carbon pool in the studied interval was linked to the salinity gradient reversal and increasing density contrast between AABW and NADW discussed above. Our reconstruction of $\delta^{13}C_{re}$ shows that this carbon pool sat below 4000 m (Figures 6g and 6h) in the Pacific and Atlantic. It seems that the high-density contrast effective prevented AABW from mixing significantly with the better ventilated NADW of high preformed $\delta^{13}C$. On one hand, the spread of the saline and dense AABW to the bottom of the Pacific and Atlantic allowed accumulation of respired carbon at abyssal sites like V28-178, 1090, and 929 (Figure 6). On the other hand, NADW can ventilate the middepth Pacific with minimal interaction with AABW, making it possible for the middepth sites, such as Sites 806, 807, and 849, to maintain their relative high $\delta^{13}C$ by counterbalancing the influence of the highly ^{13}C-depleted AABW (Figure 6). This would be in sharp contrast to the modern scenario under which NADW is more effectively mixed and transformed into LCDW in the Southern Ocean before entering the Pacific, preventing it from ventilating the middepth Pacific directly [*Talley*, 2013; *Talley et al*., 2011].

4. Conclusion

Using a collection of benthic isotope records and a $\delta^{13}C$-$\delta^{18}O$ mixing model, we uncover several large-scale features of deepwater circulation in the 2.4–1.7 Ma interval, during which the AABW-PDW $\delta^{13}C$ gradient was reversed comparing with today. Vertical structures of $\delta^{13}C$ demonstrate the presence of a ^{13}C-depleted water

mass of Southern Ocean origin extending to the bottom of the Equatorial Pacific and Equatorial Atlantic (Figure 4). Like today, vertical $\delta^{13}C$ gradient was small in the North Atlantic above 3500 m, pointing to a homogeneous NADW of high preformed $\delta^{13}C$. Above 3000 m in the Pacific, vertical profile of $\delta^{13}C$ was also essential the same as today with $\delta^{13}C$ decreasing upward to the intermediate depth, suggesting that there was no deepwater formation or enhancement of intermediate water in the studied interval. A two-end-member mixing regime between NADW and AABW is identified in the benthic $\delta^{13}C$-$\delta^{18}O$ space. The $\delta^{18}O$ of NADW was much lower than AABW, but its $\delta^{13}C$ was significantly higher (Figure 3). The distribution of m_{NADW} suggests that NADW ventilated most of the deep Pacific and deep Atlantic, while AABW only extended to the bottom of the ocean (Figure 6). Stratification of Southern Ocean deepwater masses can be clearly identified, and we also found that the maximum remineralization effect was located at the ocean bottom.

We hypothesize that the described circulation pattern was intrinsically connected to the onset of NHG. The benthic $\delta^{18}O$ gradient between AABW and NADW suggests that the initiation of stratification and reduction of ventilation in the Southern Ocean were likely due to the reversal of AABW-NADW salinity gradient linked to the expansion of sea ice [*Hillenbrand and Fütterer*, 2001; *Hillenbrand and Ehrmann*, 2005; *McKay et al*., 2012] and the reduction of southward heat transport [*Adkins*, 2013; *Woodard et al*., 2014]. Finally, our model reconstruction of carbon remineralization effect ($\delta^{13}C_{re}$) provides evidence for the argument that increasing carbon storage in the deep ocean partially drove the cooling trend that led to the onset of NHG [*Hodell and Venz-Curtis*, 2006; *Waddell et al*., 2009].

Acknowledgments

The early Pleistocene benthic isotopic data of ODP 807 generated by this study are available in Data Set S1 in the supporting information. This research is supported by the National Natural Science Foundation of China (grant41376043). We thank the Ocean Drilling Program (ODP) for providing sediment samples and the State Key Laboratory of Marine Geology at Tongji University for carrying out benthic foraminiferal stable isotopic analyses. We express gratitude to all the colleagues, particularly Torsten Bickert and Lorraine Lisiecki, for making their data available through either personal communication or online database. We are also grateful to Heiko Pälike for editorial handling and two anonymous reviewers for helpful comments that improved our manuscript.

References

Adkins, J. F. (2013), The role of deep ocean circulation in setting glacial climates, *Paleoceanography*, *28*, 539–561, doi:10.1002/palo.20046.

Adkins, J. F., K. McIntyre, and D. P. Schrag (2002), The salinity, temperature, and $\delta^{18}O$ of the glacial deep ocean, *Science*, *298*(5599), 1769–1773, doi:10.1126/science.1076252.

Bartoli, G., B. Hönisch, and R. E. Zeebe (2011), Atmospheric CO_2 decline during the Pliocene intensification of Northern Hemisphere glaciations, *Paleoceanography*, *26*, PA4213, doi:10.1029/2010PA002055.

Barton, C. E., and J. Bloemendal (1995), Paleomagnetism of sediments collected during Leg 90, Southwest Pacific, in *Init. Repts. DSDP, 90*, edited by J. P. Kennett et al., pp. 1273–1316, Ocean Drilling Program, Washington, (U.S. Govt. Printing Office), doi:10.2973/dsdp.proc.90.136.1986.

Belanger, P. E., W. B. Curry, and R. K. Matthews (1981), Core-top evaluation of benthic foraminiferal isotopic ratios for paleo-oceanographic interpretations, *Palaeogeogr. Palaeoclimatol. Palaeoecol.*, *33*(1–3), 205–220, doi:10.1016/0031-0182(81)90039-0.

Bell, D. B., S. J. A. Jung, and D. Kroon (2015), The Plio-Pleistocene development of Atlantic deep-water circulation and its influence on climate trends, *Quat. Sci. Rev.*, *123*, 265–282.

Bickert, T., W. B. Curry, and G. Wefer (1997), Late Pliocene to Holocene (2.6–0 Ma) western equatorial Atlantic deep-water circulation: Inferences from benthic stable isotopes, in *Proc. ODP, Sci. Results, 154*, edited by N. J. Shackleton et al., pp. 239–253, Ocean Drilling Program, College Station, Tex., doi:10.2973/odp.proc.sr.154.110.1997.

Bostock, H. C., B. N. Opdyke, and M. J. M. Williams (2010), Characterising the intermediate depth waters of the Pacific Ocean using $\delta^{13}C$ and other geochemical tracers, *Deep Sea Res., Part I*, *57*(7), 847–859, doi:10.1016/j.dsr.2010.04.005.

Brierley, C. M., and A. V. Fedorov (2010), Relative importance of meridional and zonal sea surface temperature gradients for the onset of the ice ages and Pliocene-Pleistocene climate evolution, *Paleoceanography*, *25*, PA2214, doi:10.1029/2009PA001809.

Broecker, W. S. (1997), Thermohaline circulation, the Achilles heel of our climate system: Will man-made CO2 upset the current balance?, *Science*, *278*(5343), 1582–1588, doi:10.1126/science.278.5343.1582.

Broecker, W. S. (2003), Does the trigger for abrupt climate change reside in the ocean or in the atmosphere?, *Science*, *300*(5625), 1519–1522, doi:10.1126/science.1083797.

Broecker, W. S., and E. Maier-Reimer (1992), The influence of air and sea exchange on the carbon isotope distribution in the sea, *Global Biogeochem. Cycles*, *6*(3), 315–320, doi:10.1029/92GB01672.

Cheng, X., J. Tian, and P. Wang (2004a), Data report: Stable isotopes from Site 1143, in *Proc. ODP, Sci. Results, 184*, edited by W. L. Prell et al., pp. 1–8, Ocean Drilling Program, College Station, Tex., doi:10.2973/odp.proc.sr.184.221.2004.

Cheng, X. R., Q. Zhao, J. Wang, Z. Jian, P. Xia, B. Huang, D. Fang, J. Xu, Z. Zhou, and P. Wang (2004b), Data report: Stable isotopes from Sites 1147 and 1148, in *Proc. ODP, Sci. Results, 184*, edited by W. L. Prell et al., pp. 1–12, Ocean Drilling Program, College Station, Tex., doi:10.2973/odp.proc.sr.184.223.2004.

Clark, P. U., N. G. Pisias, T. F. Stocker, and A. J. Weaver (2002), The role of the thermohaline circulation in abrupt climate change, *Nature*, *415*(6874), 863–869.

Clemens, S. C., W. L. Prell, Y. Sun, Z. Liu, and G. Chen (2008), Southern Hemisphere forcing of Pliocene $\delta^{18}O$ and the evolution of Indo-Asian monsoons, *Paleoceanography*, *23*, PA4210, doi:10.1029/2008PA001638.

Curry, W. B., and K. G. Miller (1989), Oxygen and carbon isotopic variation in Pliocene benthic foraminiferas of the equatorial Atlantic, in *Proc. ODP, Sci. Results, 108*, edited by W. Ruddiman et al., pp. 157–166, Ocean Drilling Program, College Station, Tex., doi:10.2973/odp.proc.sr.138.160.1995.

de Brauwere, A., S. H. M. Jacquet, F. De Ridder, F. Dehairs, R. Pintelon, J. Schoukens, and W. Baeyens (2007), Water mass distributions in the Southern Ocean derived from a parametric analysis of mixing water masses, *J. Geophys. Res.*, *112*, C02021, doi:10.1029/2006JC003742.

DeVries, T., and F. Primeau (2011), Dynamically and observationally constrained estimates of water-mass distributions and ages in the global ocean, *J. Phys. Oceanogr.*, *41*(12), 2381–2401, doi:10.1175/JPO-D-10-05011.1.

Dowsett, H. J., M. M. Robinson, and K. M. Foley (2009), Pliocene three-dimensional global ocean temperature reconstruction, *Clim. Past*, *5*(4), 769–783, doi:10.5194/cp-5-769-2009.

Duplessy, J.-C., L. Labeyrie, and C. Waelbroeck (2002), Constraints on the ocean oxygen isotopic enrichment between the Last Glacial Maximum and the Holocene: Paleoceanographic implications, *Quat. Sci. Rev.*, *21*(1–3), 315–330.

Elderfield, H., P. Ferretti, M. Greaves, S. Crowhurst, I. N. McCave, D. Hodell, and A. M. Piotrowski (2012), Evolution of ocean temperature and ice volume through the mid-Pleistocene climate transition, *Science*, *337*(6095), 704–709, doi:10.1126/science.1221294.

Elmstrom, K. M., and J. P. Kennett (1986), Late Neogene paleoceanographic evolution of site 590: Southwest Pacific, in *Init. Repts. DSDP, 90*, edited by J. P. Kennett et al., pp. 371–412, Ocean Drilling Program, Washington, (U.S. Government Printing Office), doi:10.2973/dsdp.proc.90.141.1986.

Emile-Geay, J., M. A. Cane, N. Naik, R. Seager, A. C. Clement, and A. van Geen (2003), Warren revisited: Atmospheric freshwater fluxes and "Why is no deep water formed in the North Pacific", *J. Geophys. Res.*, *108*(C6), 3178, doi:10.1029/2001JC001058.

Etourneau, J., R. Schneider, T. Blanz, and P. Martinez (2010), Intensification of the Walker and Hadley atmospheric circulations during the Pliocene–Pleistocene climate transition, *Earth Planet. Sci. Lett.*, *297*(1–2), 103–110, doi:10.1016/j.epsl.2010.06.010.

Fedorov, A. V., C. M. Brierley, K. T. Lawrence, Z. Liu, P. S. Dekens, and A. C. Ravelo (2013), Patterns and mechanisms of early Pliocene warmth, *Nature*, *496*(7443), 43–49, doi:10.1038/nature12003.

Gebbie, G. (2012), Tracer transport timescales and the observed Atlantic-Pacific lag in the timing of the Last Termination, *Paleoceanography*, *27*, PA3225, doi:10.1029/2011PA002273.

Gebbie, G. (2014), How much did Glacial North Atlantic Water shoal?, *Paleoceanography*, *29*, 190–209, doi:10.1002/2013PA002557.

Gebbie, G., and P. Huybers (2006), Meridional circulation during the Last Glacial Maximum explored through a combination of South Atlantic $\delta^{18}O$ observations and a geostrophic inverse model, *Geochem. Geophys. Geosyst.*, *7*, Q11N07, doi:10.1029/2006GC001383.

Gebbie, G., and P. Huybers (2010), Total matrix intercomparison: A method for determining the geometry of water-mass pathways, *J. Phys. Oceanogr.*, *40*(8), 1710–1728, doi:10.1175/2010JPO4272.1.

Gebbie, G., G. J. Streletz, and H. J. Spero (2016), How well would modern-day oceanic property distributions be known with paleoceanographic-like observations?, *Paleoceanography*, *31*, 472–490, doi:10.1002/2015PA002917.

Gradstein, F. M., J. G. Ogg, M. D. Schmitz, and G. M. Ogg (2012), *The Geologic Time Scale*, pp. 1083–1128, Elsevier, Boston.

Graham, D. W., B. H. Corliss, M. L. Bender, and L. D. Keigwin Jr. (1981), Carbon and oxygen isotopic disequilibria of recent deep-sea benthic foraminifera, *Mar. Micropaleontol.*, *6*(5–6), 483–497, doi:10.1016/0377-8398(81)90018-9.

Harris, S. E. (2002), Data report: Late Pliocene–Pleistocene carbon and oxygen stable isotopes from benthic foraminifers at Ocean Drilling Program Site 1123 in the southwest Pacific, in *Proc. ODP, Sci. Results, 181*, edited by C. Richter, pp. 1–20, Ocean Drilling Program, College Station, Tex., doi:10.2973/odp.proc.sr.181.203.2002.

Haug, G. H., and R. Tiedemann (1998), Effect of the formation of the Isthmus of Panama on Atlantic Ocean thermohaline circulation, *Nature*, *393*(6686), 673–676.

Haug, G. H., D. M. Sigman, R. Tiedemann, T. F. Pedersen, and M. Sarnthein (1999), Onset of permanent stratification in the subarctic Pacific Ocean, *Nature*, *401*(6755), 779–782, doi:10.1038/44550.

Hillenbrand, C.-D., and W. Ehrmann (2005), Late Neogene to Quaternary environmental changes in the Antarctic Peninsula region: Evidence from drift sediments, *Global Planet. Change*, *45*, 165–191, doi:10.1016/j.gloplacha.2004.09.006.

Hillenbrand, C.-D., and D. K. Fütterer (2001), Neogene to Quaternary deposition of opal on the continental rise west of the Antarctic Peninsula, ODP Leg 178, Sites 1095, 1096, and 1101, in *Proc. ODP, Sci. Results, 178*, edited by P. F. Barker et al., pp. 1–33, Ocean Drilling Program, College Station, Tex., doi:10.2973/odp.proc.sr.178.215.2001.

Hodell, D. A., and K. A. Venz-Curtis (2006), Late Neogene history of deepwater ventilation in the Southern Ocean, *Geochem. Geophys. Geosyst.*, *7*, Q09001, doi:10.1029/2005GC001211.

Hodell, D. A., and K. Venz (1992), Toward a high-resolution stable isotopic record of the Southern Ocean during the Pliocene-Pleistocene (4.8 to 0.8 MA), in *The Antarctic Paleoenvironment: A Perspective on Global Change: Part One*, pp. 265–310, AGU, Washington, doi:10.1029/AR056p0265.

Hodell, D. A., K. A. Venz, C. D. Charles, and U. S. Ninnemann (2003a), Pleistocene vertical carbon isotope and carbonate gradients in the South Atlantic sector of the Southern Ocean, *Geochem. Geophys. Geosyst.*, *4*(1), 1004, doi:10.1029/2002GC000367.

Hodell, D. A., C. D. Charles, J. H. Curtis, P. G. Mortyn, U. S. Ninnemann, and K. A. Venz (2003b), Data report: Oxygen isotope stratigraphy of ODP Leg 177 Sites 1088, 1089, 1090, 1093, and 1094, paper presented at Proc. Ocean Drill. Program Sci. Results.

Huybers, P., G. Gebbie, and O. Marchal (2007), Can paleoceanographic tracers constrain meridional circulation rates?, *J. Phys. Oceanogr.*, *37*(2), 394–407, doi:10.1175/JPO3018.1.

Isern, A. R., J. A. McKenzie, and D. W. Müller (1993), Paleoceanographic changes and reef growth off the northeastern Australian margin: Stable isotopic data from Leg 133, Sites 811 and 817, and Leg 21, Site 209, in *Proc. ODP, Sci. Results, 133*, edited by J. A. McKenzie et al., pp. 263–280, Ocean Drilling Program, College Station, Tex., doi:10.2973/odp.proc.sr.133.230.1993.

Jin, H., Z. Jian, X. Cheng, and J. Guo (2011), Early Pleistocene formation of the asymmetric east-west pattern of upper water structure in the equatorial Pacific Ocean, *Chin. Sci. Bull.*, *56*(21), 2251–2257, doi:10.1007/s11434-011-4547-3.

Johnson, G. C. (2008), Quantifying Antarctic Bottom Water and North Atlantic Deep Water volumes, *J. Geophys. Res.*, *113*, C05027, doi:10.1029/2007JC004477.

Karas, C., D. Nurnberg, A. K. Gupta, R. Tiedemann, K. Mohan, and T. Bickert (2009), Mid-Pliocene climate change amplified by a switch in Indonesian subsurface throughflow, *Nat. Geosci.*, *2*(6), 434–438, doi:10.1038/ngeo520.

Kawabe, M., and S. Fujio (2010), Pacific Ocean circulation based on observation, *J. Oceanogr.*, *66*(3), 389–403, doi:10.1007/s10872-010-0034-8.

Key, R. M., A. Kozyr, C. L. Sabine, K. Lee, R. Wanninkhof, J. L. Bullister, R. A. Feely, F. J. Millero, C. Mordy, and T. H. Peng (2004), A global ocean carbon climatology: Results from Global Data Analysis Project (GLODAP), *Global Biogeochem. Cycles*, *18*, GB4031, doi:10.1029/2004GB002247.

Khatiwala, S., F. Primeau, and M. Holzer (2012), Ventilation of the deep ocean constrained with tracer observations and implications for radiocarbon estimates of ideal mean age, *Earth Planet. Sci. Lett.*, *325–326*, 116–125, doi:10.1016/j.epsl.2012.01.038.

Knox, F., and M. B. McElroy (1984), Changes in atmospheric CO_2: Influence of the marine biota at high latitude, *J. Geophys. Res.*, *89*(D3), 4629–4637, doi:10.1029/JD089iD03p04629.

Kroopnick, P. M. (1985), The distribution of ^{13}C of ΣCO_2 in the world oceans, *Deep Sea Res. Part A. Oceanogr. Res. Pap.*, *32*(1), 57–84, doi:10.1016/0198-0149(85)90017-2.

Kwiek, P. B., and A. C. Ravelo (1999), Pacific Ocean intermediate and deep water circulation during the Pliocene, *Palaeogeogr. Palaeoclimatol. Palaeoecol.*, *154*(3), 191–217, doi:10.1016/S0031-0182(99)00111-X.

LeGrand, P., and C. Wunsch (1995), Constraints from paleotracer data on the North Atlantic circulation during the Last Glacial Maximum, *Paleoceanography*, *10*(6), 1011–1045, doi:10.1029/95PA01455.
LeGrande, A. N., and G. A. Schmidt (2006), Global gridded data set of the oxygen isotopic composition in seawater, *Geophys. Res. Lett.*, *33*, L12604, doi:10.1029/2006GL026011.
Lisiecki, L. E. (2010), A simple mixing explanation for late Pleistocene changes in the Pacific-South Atlantic benthic $\delta^{13}C$ gradient, *Clim. Past*, *6*(3), 305–314, doi:10.5194/cp-6-305-2010.
Lisiecki, L. E. (2014), Atlantic overturning responses to obliquity and precession over the last 3 Myr, *Paleoceanography*, *29*, 71–86, doi:10.1002/2013PA002505.
Lisiecki, L. E., and P. A. Lisiecki (2002), Application of dynamic programming to the correlation of paleoclimate records, *Paleoceanography*, *17*(4), 1049, doi:10.1029/2001PA000733.
Lisiecki, L. E., and M. E. Raymo (2005), A Pliocene-Pleistocene stack of 57 globally distributed benthic $\delta^{18}O$ records, *Paleoceanography*, *20*, PA1003, doi:10.1029/2004PA001071.
Lynch-Stieglitz, J. (2003), Tracers of past ocean circulation, in *Treatise on Geochemistry*, edited by H. D. Holland and K. K. Turekian, pp. 433–451, Pergamon, Oxford, doi:10.1016/B0-08-043751-6/06117-X.
MacCready, P., W. E. Johns, C. G. Rooth, D. M. Fratantoni, and R. A. Watlington (1999), Overflow into the deep Caribbean: Effects of plume variability, *J. Geophys. Res.*, *104*(C11), 25,913–25,935, doi:10.1029/1999JC900206.
Mackensen, A., H. W. Hubberten, T. Bickert, G. Fischer, and D. K. Fütterer (1993), The $\delta^{13}C$ in benthic foraminiferal tests of *Fontbotia wuellerstorfi* (Schwager) relative to the $\delta^{13}C$ of dissolved inorganic carbon in Southern Ocean Deep Water: Implications for glacial ocean circulation models, *Paleoceanography*, *8*(5), 587–610, doi:10.1029/93PA01291.
Marchal, O., and W. B. Curry (2008), On the abyssal circulation in the glacial Atlantic, *J. Phys. Oceanogr.*, *38*(9), 2014–2037, doi:10.1175/2008JPO3895.1.
Marchitto, T. M., W. B. Curry, J. Lynch-Stieglitz, S. P. Bryan, K. M. Cobb, and D. C. Lund (2014), Improved oxygen isotope temperature calibrations for cosmopolitan benthic foraminifera, *Geochim. Cosmochim. Acta*, *130*, 1–11, doi:10.1016/j.gca.2013.12.034.
Martinez-Boti, M. A., G. L. Foster, T. B. Chalk, E. J. Rohling, P. F. Sexton, D. J. Lunt, R. D. Pancost, M. P. S. Badger, and D. N. Schmidt (2015), Plio-Pleistocene climate sensitivity evaluated using high-resolution CO2 records, *Nature*, *518*(7537), 49–54, doi:10.1038/nature14145.
McCorkle, D. C., and L. D. Keigwin (1994), Depth profiles of $\delta^{13}C$ in bottom water and core top *C. wuellerstorfi* on the Ontong Java Plateau and Emperor Seamounts, *Paleoceanography*, *9*(2), 197–208, doi:10.1029/93PA03271.
McKay, R., et al. (2012), Antarctic and Southern Ocean influences on Late Pliocene global cooling, *Proc. Natl. Acad. Sci. U.S.A.*, *109*(17), 6423–6428, doi:10.1073/pnas.1112248109.
Mix, A. C., J. Le, and N. J. Shackleton (1995a), Benthic foraminiferal stable isotope stratigraphy of Site 846: 0–1.8 Ma, in *Proc. ODP, Sci. Results, 138*, edited by N. G. Pisias et al., pp. 839–854, Ocean Drilling Program, College Station, Tex., doi:10.2973/odp.proc.sr.138.160.1995.
Mix, A. C., N. G. Pisias, W. Rugh, J. Wilson, A. Morey, and T. K. Hagelberg (1995b), Benthic foraminifer stable isotope record from Site 849 (0–5 Ma): Local and global climate changes, in *Proc. ODP, Sci. Results, 138*, edited by N. G. Pisias et al., pp. 371–412, Ocean Drilling Program, College Station, Tex., doi:10.2973/odp.proc.sr.138.120.1995.
Mudelsee, M., and M. E. Raymo (2005), Slow dynamics of the Northern Hemisphere glaciation, *Paleoceanography*, *20*, PA4022, doi:10.1029/2005PA001153.
Oppo, D. W., and R. G. Fairbanks (1987), Variability in the deep and intermediate water circulation of the Atlantic Ocean during the past 25,000 years: Northern Hemisphere modulation of the Southern Ocean, *Earth Planet. Sci. Lett.*, *86*(1), 1–15, doi:10.1016/0012-821X(87)90183-X.
Ostermann, D. R., and W. B. Curry (2000), Calibration of stable isotopic data: An enriched δ18O standard used for source gas mixing detection and correction, *Paleoceanography*, *15*(3), 353–360, doi:10.1029/1999PA000411.
Poole, R., and M. Tomczak (1999), Optimum multiparameter analysis of the water mass structure in the Atlantic Ocean thermocline, *Deep Sea Res., Part I*, *46*(11), 1895–1921, doi:10.1016/S0967-0637(99)00025-4.
Rahmstorf, S. (2002), Ocean circulation and climate during the past 120,000 years, *Nature*, *419*(6903), 207–214.
Raymo, M. E. (1994), The initiation of Northern Hemisphere glaciation, *Annu. Rev. Earth Planet. Sci.*, *22*(1), 353–383, doi:10.1146/annurev.ea.22.050194.002033.
Raymo, M. E., W. F. Ruddiman, J. Backman, B. M. Clement, and D. G. Martinson (1989), Late Pliocene variation in northern hemisphere ice sheets and North Atlantic deep water circulation, *Paleoceanography*, *4*(4), 413–446, doi:10.1029/PA004i004p00413.
Raymo, M. E., W. F. Ruddiman, N. J. Shackleton, and D. W. Oppo (1990), Evolution of Atlantic-Pacific $\delta^{13}C$ gradients over the last 2.5 m.y, *Earth Planet. Sci. Lett.*, *97*(3–4), 353–368, doi:10.1016/0012-821X(90)90051-X.
Raymo, M. E., D. Hodell, and E. Jansen (1992), Response of deep ocean circulation to initiation of northern hemisphere glaciation (3–2 MA), *Paleoceanography*, *7*(5), 645–672, doi:10.1029/92PA01609.
Raymo, M. E., D. W. Oppo, B. P. Flower, D. A. Hodell, J. F. McManus, K. A. Venz, K. F. Kleiven, and K. McIntyre (2004), Stability of North Atlantic water masses in face of pronounced climate variability during the Pleistocene, *Paleoceanography*, *19*, PA2008, doi:10.1029/2003PA000921.
Rintoul, S. R., W. C. Hughes, and D. Olbers (2001), The Antarctic Circumpolar Current System, in *International Geophysics*, edited by G. Siedler, J. Church and J. Gould, pp. 271–302, Academic Press, Amsterdam, doi:10.1016/S0074-6142(01)80124-8.
Sarmiento, J. L., and J. R. Toggweiler (1984), A new model for the role of the oceans in determining atmospheric pCO_2, *Nature*, *308*(5960), 621–624, doi:10.1038/308621a0.
Sarnthein, M., G. Bartoli, M. Prange, A. Schmittner, B. Schneider, M. Weinelt, N. Andersen, and D. Garbe-Schönberg (2009), Mid-Pliocene shifts in ocean overturning circulation and the onset of Quaternary-style climates, *Clim. Past*, *5*(2), 269–283, doi:10.5194/cp-5-269-2009.
Schlitzer, R. (2014), Ocean Data View. [Available at http://odv.awi.de.]
Schmittner, A., N. Gruber, A. C. Mix, R. M. Key, A. Tagliabue, and T. K. Westberry (2013), Biology and air-sea gas exchange controls on the distribution of carbon isotope ratios ($\delta^{13}C$) in the ocean, *Biogeosciences*, *10*(9), 5793–5816, doi:10.5194/bg-10-5793-2013.
Shackleton, N. J., and M. A. Hall (1984), Oxygen and carbon isotope stratigraphy of Deep Sea Drilling Project Hole 552A: Plio-Pleistocene glacial history, in *Init. Repts. DSDP, 81*, edited by D. G. Roberts et al., pp. 337–355, Ocean Drilling Program, Washington, (U.S. Goverment Printing Office), doi:10.2973/dsdp.proc.81.116.1984.
Shackleton, N. J., and N. D. Opdyke (1977), Oxygen isotope and palaeomagnetic evidence for early Northern Hemisphere glaciation, *Nature*, *270*(5634), 216–219.
Siegenthaler, U., and T. Wenk (1984), Rapid atmospheric CO_2 variations and ocean circulation, *Nature*, *308*(5960), 624–626, doi:10.1038/308624a0.

Sigman, D. M., and E. A. Boyle (2000), Glacial/interglacial variations in atmospheric carbon dioxide, *Nature*, *407*(6806), 859–869, doi:10.1038/35038000.
Sigman, D. M., S. L. Jaccard, and G. H. Haug (2004), Polar ocean stratification in a cold climate, *Nature*, *428*(6978), 59–63, doi:10.1038/nature02357.
Sosdian, S., and Y. Rosenthal (2009), Deep-sea temperature and ice volume changes across the Pliocene-Pleistocene climate transitions, *Science*, *325*(5938), 306–310, doi:10.1126/science.1169938.
Swann, G. E. A. (2010), Salinity changes in the North West Pacific Ocean during the late Pliocene/early Quaternary from 2.73 Ma to 2.52 Ma, *Earth Planet. Sci. Lett.*, *297*(1–2), 332–338, doi:10.1016/j.epsl.2010.06.035.
Talley, L. D. (2013), Closure of the global overturning circulation through the Indian, Pacific, and Southern Oceans: Schematics and transports, *Oceanography*, *21*(1), 80–97, doi:10.5670/oceanog.2013.07.
Talley, L. D., G. L. Pickard, W. J. Emery, and J. H. Swift (2011), *Descriptive Physical Oceanography: An Introduction*, 6th ed., 560 pp., Elsevier, Boston.
Tian, J., Q. Zhao, P. Wang, Q. Li, and X. Cheng (2008), Astronomically modulated Neogene sediment records from the South China Sea, *Paleoceanography*, *23*, PA3210, doi:10.1029/2007PA001552.
Venti, N. L., and K. Billups (2012), Stable-isotope stratigraphy of the Pliocene–Pleistocene climate transition in the northwestern subtropical Pacific, *Palaeogeogr. Palaeoclimatol. Palaeoecol.*, *326–328*, 54–65, doi:10.1016/j.palaeo.2012.02.001.
Venz, K. A., and D. A. Hodell (2002), New evidence for changes in Plio–Pleistocene deep water circulation from Southern Ocean ODP Leg 177 Site 1090, *Palaeogeogr. Palaeoclimatol. Palaeoecol.*, *182*(3–4), 197–220, doi:10.1016/S0031-0182(01)00496-5.
Waddell, L. M., I. L. Hendy, T. C. Moore, and M. W. Lyle (2009), Ventilation of the abyssal Southern Ocean during the late Neogene: A new perspective from the subantarctic Pacific, *Paleoceanography*, *24*, PA3206, doi:10.1029/2008PA001661.
Wang, P., and Q. Li (2009), Oceanographical and geological background, in *The South China Sea*, edited by P. Wang and Q. Li, pp. 25–73, Springer, Netherlands, doi:10.1007/978-1-4020-9745-4_2.
Wara, M. W., A. C. Ravelo, and M. L. Delaney (2005), Permanent El Niño-like conditions during the Pliocene warm period, *Science*, *309*(5735), 758–761, doi:10.1126/science.1112596.
Warren, B. A. (1983), Why is no deep water formed in the North Pacific?, *J. Mar. Res.*, *41*(2), 327–347, doi:10.1357/002224083788520207.
Whitman, J. M., and W. H. Berger (1993), Pliocene-Pleistocene carbon isotope record, Site 586, Ontong Java Plateau, in *Proc. ODP, Sci. Results, 130*, edited by W. H. Berger et al., pp. 333–348, Ocean Drilling Program, College Station, Tex., doi:10.2973/odp.proc.sr.130.030.1993.
Woodard, S. C., Y. Rosenthal, K. G. Miller, J. D. Wright, B. K. Chiu, and K. T. Lawrence (2014), Antarctic role in Northern Hemisphere glaciation, *Science*, *346*(6211), 847–851, doi:10.1126/science.1255586.
Wunsch, C. (2006), *Discrete Inverse and State Estimation Problems: With Geophysical Fluid Applications*, Cambridge Univ. Press, Cambrige, U. K.
Zahn, R., and A. C. Mix (1991), Benthic foraminiferal $\delta^{18}O$ in the ocean's temperature-salinity-density field: Constraints on Ice Age thermohaline circulation, *Paleoceanography*, *6*(1), 1–20, doi:10.1029/90PA01882.
Zahn, R., K. Winn, and M. Sarnthein (1986), Benthic foraminiferal $\delta^{13}C$ and accumulation rates of organic carbon: *Uvigerina Peregrina* group and *Cibicidoides Wuellerstorfi*, *Paleoceanography*, *1*(1), 27–42, doi:10.1029/PA001i001p00027.
Zhang, J., P. Wang, Q. Li, X. Cheng, H. Jin, and S. Zhang (2007), Western equatorial Pacific productivity and carbonate dissolution over the last 550 kyr: Foraminiferal and nannofossil evidence from ODP Hole 807A, *Mar. Micropaleontol.*, *64*(3–4), 121–140, doi:10.1016/j.marmicro.2007.03.003.